SPECIFICITY OF TLS11a APTAMER TOWARDS HEPATOCELLULAR CARCINOMA AS A MEANS OF DETECTION AND TARGETED DRUG DELIVERY

by

Katie Addilynn Kendrick, B.S.

A thesis submitted to the Graduate Council of
Texas State University in partial fulfillment
of the requirements for the degree of
Master of Science,
with a Major in Biology
August 2017

Committee Members:

Shannon Weigum, Chair

Dana García

Joe Koke

FAIR USE AND AUTHORS'S PERMISSION STATEMENT

Fair Use

Duplication Permission

DEDICATION

I would like to dedicate this work to my children and my loving family for all their continuous love and support throughout this journey. Most importantly, I would like to thank my children, Kaydence and Drake, for being such amazing individuals and being understanding of my demanding schedule. There were many times they had to let me work when they wanted to be doing other things. No matter how exhausted I was or how many times I wanted to give up, I continued to push myself so they could see their mother succeed and so they know that their education is important. They are the reason I continue to reach for the stars.

I would also like to dedicate this work to my family and friends, I will always be appreciative of your everlasting encouragement and support. I would not have been able to complete this adventure without the support and guidance from my amazing mother and best friend, Linda, my father, Mickey, and second father, Louis. Not only did they do a wonderful job raising me but they have also helped raise my children and took on many responsibilities to help me complete my goal. I would like to thank my fiancé, David, for supporting me and making sure I did not give up along the way. You have always believed in me and all my dreams. Also, I'd like to thank my sister, Lindsey, for being there in times of need, especially the last few weeks, and always encouraging me to do my best. Lastly, I'd like to thank the rest of my family and friends for their encouragement, love and support. I love you all.

ACKNOWLEDGMENTS

I would like to thank Dr. Shannon Weigum for giving me the amazing opportunity of working in her lab. I know at times it was difficult to juggle my research and my children however, she was always helpful, accepting and willing to work around my schedule. She was always there to listen and provide direction when I was stuck and more importantly had faith in me and pushed me to continue when I had lost all hope. Her mentorship has taught me many life lessons, not only in the lab but also for future endeavors. I will always be grateful for her support and thankful that she helped me succeed in achieving my goal.

I would like to thank Ms. Alissa Savage who works at the Analysis Research Service Center for the many hours spent assisting me with the confocal microscopy training and answering my many questions. I want to thank Dr. Tania Betancourt for allowing me to use her CY7 filter cube on many occasions. I also thank my committee members Dr. Dana García and Dr. Joe Koke.

Additionally, I would like to thank my former and current lab members Melissa Sutton, Lichen Xiang, Kshitij Ranjan, Zhenyuan Lu, Elizabeth McIvor, and Kelly Braddock for their support and open ears.

This work was supported by funding provided by Texas State University and the Research Enhancement Program.

TABLE OF CONTENTS

Page

LIST OF TABLES

Table **Page**

LIST OF FIGURES

Figure **Page**

LIST OF ABBREVIATIONS

Abbreviation	Description
AF	Autofluorescence
BSA	Bovine serum albumin
CL.2	Normal liver mouse cell line
DAB	Diaminobenzidine substrate
FBS	Fetal bovine serum
FF	Fresh frozen
FFPE	Formalin fixed paraffin embedded
HCC	Hepatocellular carcinoma
IHC	Immunohistochemistry
MEAR	HCC mouse cell line
NIR	Near infrared
PBS	Phosphate buffered saline
PBSA	0.1% BSA in PBS
ROI	Region of interest
SELEX	Systematic Evolution of Ligands by EXponential enrichment
TMA	Tissue microarray

ABSTRACT

Liver cancer is the sixth most commonly occurring cancer and second leading cause of cancer-related deaths worldwide with an estimated 75% of all liver malignancy cases being hepatocellular carcinoma (HCC), the most common and most lethal form of liver cancer [1]. While the incidence rates for many cancers have slowly declined over the years, HCC incidence and death rates have been continuously rising due to late stage diagnoses and poor prognoses. This suggests that there is a lack of existing biomarkers and diagnostic equipment sensitive enough to identify this disease in early stages [2]. More sophisticated methods are needed to detect HCC in early stages and specifically target this disease. Recently, an HCC-specific aptamer was created and shown to effectively discriminate mouse HCC from normal liver *in vitro* [3]. In this thesis, the specificity of TLS11a towards HCC is addressed regarding human tissue. Specifically, immunohistochemical (IHC) staining of human tissue microarrays (TMA) was utilized to address what tissue types TLS11a can bind, if it can differentiate between normal liver and HCC tissue and if binding is correlated with tumor stage. Formalin fixed paraffin embedded (FFPE) TMAs were stained with fluorophore labeled TLS11a and imaged using epifluorescence microscopy. However, negative controls demonstrated high levels of autofluorescence (AF) which made aptamer-based fluorescence indistinguishable from background. Attempts to induce aptamer refolding, antigen retrieval and using alternate fluorophores were unsuccessful at increasing the signal to noise ratio. Colorimetric FFPE staining was also pursued; unfortunately, there was no indication of aptamer binding

above background using these conditions either. Ultimately, this lack of specific binding between TLS11a and HCC tissue was attributed to disruption or loss of cell surface binding sites and epitopes during the formalin fixation and paraffin embedding process. Using immunofluorescence staining of fresh frozen (FF) TMAs, TLS11a was found to effectively distinguish between normal liver and HCC tissue ($p<0.001$) in human tissue with the mean integrated intensity increasing more than 10-fold on average in HCC tissues. TLS11a was also found to bind to other malignant tissue types including breast, lung, kidney and colon, among others, with little to no binding to normal tissues ($p<0.0001$). These results signify that TLS11a has the potential to be used for targeting multiple malignancies. Additional studies are needed to confirm these findings; however, these studies suggest TLS11a has the potential to be a tumor-specific marker, particularly with respect to HCC, and would be an excellent candidate for use in human studies for new HCC-targeted diagnostic and therapeutic applications.

1. INTRODUCTION

Cancer is a major health concern, accounting for 1 in every 7 deaths worldwide, with 14.1 million new cases and 8.2 million deaths recorded in 2012 alone [4, 5]. Globally, the rate of incidence is continuing to grow at an alarming rate, with an estimated 21.7 million new cases expected to occur each year by 2030 [4]. During 2016, in the United States alone, an estimated 1,630 people succumbed to cancer per day with the total cancer-related deaths of 2016 coming in at an estimated 595,690 people, making cancer the second most common cause of death in the US [4]. Some types of cancer are caused by environmental factors and lifestyle choices, which in many cases could be prevented, while other cancer types are genetically inherited or are a result of chromosomal mutations [4, 6].

1.1. Cancer Background and Development

Cancer is a generic name for a broad assortment of diseases that cause disorderly and uncontrollable cell proliferation beginning from a single, DNA-damaged cell [4]. Normal cells proceed through the cell cycle in a coordinated and controlled manner, in which they grow, divide and die without invading other tissues or causing harm; cancer cells do not [7]. The cell cycle is composed of many checkpoints and control mechanisms to ensure that abnormal cells do not continue dividing. Checkpoints enable completion of critical phases in the cell cycle and ensure that damaged or incomplete DNA is repaired before entering the next stage [8]. If at any time these mechanisms sense a problem they can halt the cell cycle for repair, or if unable to repair, can activate genes for programed cell death [8]. Due to these cell cycle regulatory functions, most cells are resistant to chromosomal changes and are able to stop abnormal cell growth from occurring [9].

Unfortunately, these cell cycle mechanisms are not fail-safe and some cells can bypass the process and proceed to form neoplasias [9].

All cancers are different: some malignancies grow slowly while others grow more quickly; some spread to distant tissues in the body while others remain localized; some form solid tumors while others grow in the blood. However, cancer cells share certain traits that are known as hallmarks [10]. The hallmarks of cancer are the general characteristics that most cancer-forming cells can acquire through the process of a normal cell developing into a cancer cell. Such hallmarks include the ability to achieve sustained proliferative signaling, evade growth suppressors and immune destruction, acquire replicative immortality, induce tumor-promoting growth environments through angiogenesis (formation of new blood vessels), induce invasion and metastasis (spread from its primary location to other tissues), deregulate cellular energetics, create genome instability and resist cell death [10]. These fundamental elements are important in understanding the pathway normal cells take in becoming cancerous and can also help researchers better understand ways to prevent or treat these diseases.

1.2. Current Detection Methods and Staging

Cancer can be diagnosed by many methods including magnetic resonance imaging (MRI), X-rays, ultrasound, computed tomography (CT), positron emission tomography (PET) and testing for specific biomarkers that are indicative of a specific disease [11]. The best chances for survival is early detection. Physicians use staging, a system designed to describe the cancer's growth and spread, at diagnosis [12]. The stage at which a patient is diagnosed is important in data registries and also influences what treatment options will be most applicable to the patient [12]. The most commonly used

staging system assigns a number from 0 to 4, 0 being the lowest stage, indicating localized cancer that has not spread, and 4 being the highest stage, indicating cancers in the most advanced disease state [4, 12]. Another way to stage tumors is the TNM system, which assigns a letter (T, N or M) based on the spread of the tumor, T meaning a localized tumor, N meaning some spread to lymph nodes and M indicating metastasis [12]. Treatment options, frequently determined by tumor stage, can consist of surgical removal of the tumor, radiation, chemotherapy or a combination of these methods [4]. Some cancer types have a worse prognosis than others; however, the cancer type, stage at diagnosis, and treatment method all influence the overall survival of the patient.

1.3. Liver Cancer and Hepatocellular Carcinoma

The liver is an imperative organ in the human body and is crucial for survival. The liver serves many functions that are necessary for everyday processes such as exocrine, endocrine, digestive and immune system functions. These important functions include things such as filtering the blood to rid the body of old blood cells, toxins, and harmful pathogens, synthesis of hormones and blood clotting factors, production and secretion of bile to aid in fat breakdown, metabolism and storage of essential nutrients like proteins, lipids and carbohydrates, iron, glucose and vitamins [13]. The liver processes everything consumed, whether it be solid or liquid, and therefore is important for the individual's overall health. The liver is the largest internal organ in the human body and is composed of many cell types, but the majority are referred to as hepatocytes [13]. When cells that make up the liver begin to grow uncontrollably, it is known as liver cancer.

Liver cancer is the sixth most diagnosed cancer type and second leading cause of

cancer-related deaths worldwide with an estimated 782,000 new cases and 746,000 deaths in 2012 alone [5]. Liver cancer is more common in less developed regions, and the highest rate of incidence occurs in Eastern Asia [5]. Although there are many types of diseased states, hepatocellular carcinoma is the most common type of liver malignancy, representing 75% of all liver cancer cases [1].

The risk of developing HCC is much higher in certain individuals and is influenced by gender, ethnicity and social behaviors. Liver cancer is diagnosed in men, of all ethnic backgrounds, three times more than in women [4]. HCC incidence rates are greatest amongst American Indian/Alaska Natives, Asian/Pacific Islanders and Hispanic ethnicities with black and white ethnic populations having the lowest rate of incidence [2, 14]. The most significant risk factors for HCC are hepatitis B and hepatitis C viral infections [4]. Other important risk factors include scarring of the liver (cirrhosis), alcohol abuse, diabetes, obesity, genetic disorders, tobacco use, injectable drug use, and exposure to arsenic, aflatoxins or anabolic steroids [4, 5]. Worldwide, alcohol abuse, obesity and type 2 diabetes have become increasingly more common over time and could potentially point to the increased trend in liver cancer.

Symptoms of HCC include abdominal pain, abdominal mass or swelling, weight loss, anemia, loss of appetite, and jaundice [4]. However, it is very common for individuals to show no symptoms at all or show no symptoms until the disease has spread and the prognosis is poor [4]. Patients diagnosed at early stages, before metastasis to nearby or distant organs have higher probability of survival. The 5-year survival rate for individuals diagnosed with localized, regional and distant HCC is roughly 31%, 11% and 3% respectively [2, 4]. Liver cancer screenings are recommended for high-risk patients.

However, there has been no evidence that shows early screenings lead to decreased mortality for those that are at high risk [4]. Some of the most common methods to diagnose HCC are by x-ray, ultrasound, MRI, CT, biopsy and blood tests to look at the liver functions [11, 15, 16]. Unfortunately, HCC rates are continuing to increase each year [14]. HCC treatment options are limited and become even more so when diagnosed at late stages. When HCC is diagnosed early, treatment options can include both nonsurgical and surgical methods. Cancerous cells can be burned or frozen, commonly known as ablation, tumor vasculature can be blocked from receiving nutrients, known as embolization, or the patient can undergo partial liver removal or liver transplant [15, 17]. Those diagnosed at advanced stages have even fewer options with selections of radiation, chemotherapy, targeted drug therapy, liver transplant or a combination of these choices [15, 17]. Many of these treatment methods cause harsh systematic effects that can create more suffering for the patient and often cause more problems than solutions.

HCC incidence rates continue to increase even when many cancer types have shown a decline [2, 4]. Since the 1980's, liver cancer incidence and death rates have been increasing [2, 14]. Over the past ten years, the number of new cases and new deaths in the United States has shown to increase each year by an average of 3% and 2.7%, respectively (Figure 1) [4, 14]. Although, HCC may not be highly prevalent, the continued increase of new cases and deaths shows that it is a highly lethal disease.

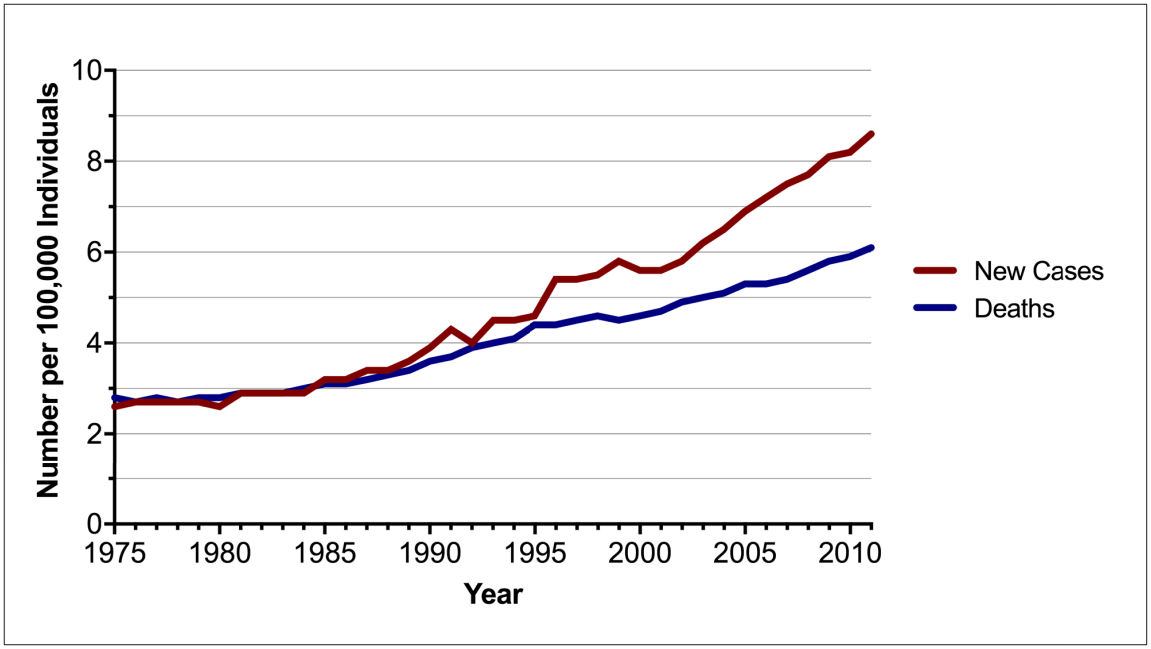

Figure 1. Age-adjusted incidence and mortality. Rates represent patients with any form of liver cancer, including HCC, from 1975 to 2013. SEER National Cancer Database.

There are many problems confronted when facing this disease. Most patients are not diagnosed until advanced stages where prognosis is poor, and many die within one year of diagnosis [1, 4]. This situation may in part be related to diagnostic techniques not being sensitive enough to detect HCC at early stages but also suggests treatment methods are ineffective. Therefore, a need remains for the advancement in our current diagnostic and therapeutic approaches to adequately identify and specifically target HCC.

1.4. Aptamers as Targeting Agents for Tumors

Aptamers are a new class of molecules composed of short nucleic acid or peptide sequences that bind to a specific target ligand with high affinity [18]. Nucleic acid aptamers are single-stranded DNA or RNA oligonucleotides, and peptide aptamers are short peptide domains attached to a protein scaffold. Aptamers, first described in the 1990s, are characterized and enriched through a process known as Systematic Evolution

of Ligands by EXponential enrichment (SELEX) [19, 20]. SELEX *in vitro* selection process begins by incubating the target of interest with a random oligonucleotide sequence library of approximately 10^{14} to 10^{15} individual molecules [20, 21]. A small amount of the random oligonucleotide pool will bind to the target and can be separated from the unbound sequences [19, 20]. Those oligonucleotides that did bind will then be isolated and amplified for a new, more enriched, library pool. Counter-selection can also be carried out by incubating sequences that were previously bound to the target with negative controls to obtain specific sequence selections [19, 20]. This same cycle of selection and amplification will continue, generally between 5-15 cycles, until affinity saturation is obtained [20, 21]. The oligonucleotides that remain are referred to as the enriched library. They and are then cloned and sequenced for identification purposes and further characterized based on their ability to bind the target successfully. The outcome of the SELEX process is full-length sequences that are typically around 70-80 nucleotides long, and if needed, can be shortened by removing nucleotides unimportant for target binding [20, 21]. The whole SELEX process takes approximately 2-3 months in order to identify the sequence of choice [20].

Single-stranded nucleic acid aptamers form complex secondary and tertiary structures. RNA aptamers can form a broader range of 3D structures and DNA aptamers tend to be more stable and less expensive than RNA aptamers [20, 21]. These aptamers are able to recognize a broad range of ligands including enzymes, growth factors, gene regulatory factors, antibodies, lectins, cell adhesion molecules, and intact viral particles [21].

Aptamers, like antibodies, bind to a specific epitope with high affinity; however,

they offer many advantages over antibodies. Antibody production occurs in animals while aptamers are produced in vitro [18, 21]. Production of aptamers is done by chemical synthesis leading to a higher degree of accuracy and reproducibility versus antibodies that could have small variations due to the fact they are made in another species [21]. Aptamers can be stored for longer periods of time, can be regenerated if denatured, have almost no immunogenicity and are better able to bind and penetrate their targets compared to antibodies [21]. Furthermore, aptamers can be chemically modified with more success and ease than antibodies. Aptamers can be modified in different positions by attaching functional groups or molecules such as fluorescent dyes or biotin for detection of *in vitro* or *in vivo* studies [18, 21]. The exceptional properties of aptamers allow them to be used in a range of applications such as biomarker identification, imaging and detection, targeted drug therapy and biosensor platforms.

A recent study showed promising results when using an aptamer specific for mucin 1 (MUC1), an epithelial tissue transmembrane protein that is overexpressed in many malignant cancers, in conjunction with near-infrared (NIR) fluorescent probes for tumor-targeting imaging applications [22]. This 25-base ssDNA aptamer, previously found to have high specificity and targeting efficacy [23], specifically targets epitopes in the variable tandem repeat regions that are exposed on MUC1 [22]. Results demonstrate, both *in vitro* and *in vivo*, that this aptamer-fluorescent probe was able to specifically target tumors with both high and low levels of MUC1 expression [22]. Another important factor in this study was the use of fluorescent molecules that are biologically safer compared to other frequently used imaging and contrast molecules [22].

Aptamers have been useful in targeting and therapeutic applications, one of which

involves the use of an aptamer, known as E3, which has been shown in mice to target prostate cancer and colon cancer, but not normal cells, *in vivo* [24]. One very interesting study showed the aptamer A8, which targets heat shock protein 70 (HSP70) on tumor-derived exosomes, could function in multiple steps involving identifying and treatment of cancer as well as the ability to increase immune responses [25]. HSP70 is a chaperone protein that participates in the activation of myeloid-derived suppressor cells (MDSCs) [25]. Unlike normal cells, HSP70 is highly overexpressed on the plasma membrane of many tumor cells [25]. MDSCs have been shown to inhibit the adaptive and innate immune response and HSP70 over-expression promotes cancer development by creating resistance to chemotherapeutic drugs [25]. Using cancer and normal patient samples with A8, researchers were able to capture and quantify HSP70 exosomes, that were found at much higher levels in cancer subjects than normal subjects ($p < 0.001$), resulting in demonstration of A8's ability to be used to detect a potential cancer biomarker [25]. A8 was also shown to block activation of MDSCs by selectively binding HSP70 and blocking its ability to interact with toll-like receptor 2 due to A8'ss higher binding affinity as shown though biosensor platforms [25]. Lastly, *in vivo* studies using mice treated with A8 and chemotherapeutic drugs showed decreased numbers of HSP70 exosomes and MDSCs and increased numbers of immune cells, thus indicating the aptamer's ability to block the harmful signaling pathway and restore immune responses [25]. Not only do these studies illustrate the ability of aptamers to bind to their target with high specificity, but also show that aptamers may be suitable for use in a wide variety of applications, including tumor detection, targeting, and treatment.

1.5. TLS11a Hepatocellular Carcinoma-specific Aptamer

A recently discovered aptamer, known as TLS11a, has been shown effective at targeting and discriminating HCC from non-cancerous liver cells of mice *in vitro* [3]. Using the whole-cell SELEX process, the TLS11a aptamer was selected against both the target mouse HCC cell line, referred to as BNL 1ME A.7R.1 (MEAR), and counter-selected against a normal mouse liver cell line, BNL CL.2 (BNL), as the negative control [3]. Initially, an ssDNA pool was incubated with MEAR target cells for 30 minutes on ice [3]. Counter-selection was done by bound DNA sequences being eluted and again incubated on ice with the BNL negative control cells creating the initial selected ssDNA pool [3]. Sequences were then amplified using PCR with FITC- or TMRA- and biotin-labeled primers and the selected sense ssDNA separated from the biotinylated antisense ssDNA strands [3]. The wash strength (wash time, volume and number of washes) was gradually increased and the addition of 20% FBS with a random 88-mer were added to decrease non-specific binding and create aptamers with high specificity and affinity toward the MEAR target cells [3]. Throughout the enrichment process, suspended cells were observed using flow cytometric analysis in order to test the aptamer binding capabilities. After 16 enrichment rounds the selected ssDNA pool was amplified using PCR and cloned into *Escherichia coli* to determine the selected aptamer sequences by Genome Sequencing Services Laboratory [3]. Seven out of 11 full length clones chosen to test were found to bind specifically to MEAR cells with high affinity [3]. After further optimization, TLS11a, a truncated version of the full-length TLS11, was found to have higher affinity toward HCC MEAR cells than any other selected aptamer: binding capacity K_d was 4.5 ± 0.4 nM [3]. TLS11a was further shown to be specific for HCC

recognition of MEAR cells by fluorescence confocal imaging. Both adherent MEAR and BNL cells were incubated with either 25 nM FITC-labeled aptamer in binding buffer or an FITC-labeled unselected DNA library and imaged [3]. Staining with TLS11a-FITC showed bright green fluorescence on the periphery of the MEAR cells and no significant fluorescence signal on BNL cells, while neither MEAR or BNL cells showed a fluorescent signal when incubated with the FITC- labeled unselected DNA library [3]. Mice were then injected with either MEAR or BNL cells, and both tumor and normal livers were removed after a period of growth [3]. Tissue was frozen and later fixed and incubated with FITC- labeled unselected DNA library or 100 nM TLS11a [3]. The results were the same as previously found, with only the frozen MEAR tumor showing a fluorescent signal when labeled with TLS11a-FITC [3]. To further demonstrate TLS11a specificity, different kinds of cell lines were tested against the aptamer. Cell lines consisted of mouse cells, MEAR and BNL, and human cell lines, three different leukemia cell lines (CCRF-CEM, Jurkat and K562), a lymphoma cell line (Ramos), a lung cancer cell line (H23), and a liver cancer cell line (Huh7) [3]. Flow cytometer results indicated TLS11a showed no significant binding to the normal mouse liver BNL, the human lymphoma cell line (Ramos) or any of the three human leukemia cell lines (CCRF-CEM, Jurkat, K562) [3]. However, there was very minor binding to the human lung cancer line, H23, with a binding capacity less than 10% and as hoped for, TLS11a showed moderate binding to the human liver cancer line, Huh7, and significant binding in the mouse HCC MEAR line [3]. Experiments from the Tan group resulted in the formation of an HCC specific aptamer with high affinity towards adherent and solid tumor cells suggesting, TLS11a has the potential to be used for HCC detection and treatment [3].

TLS11a has also been shown effective in a biosensor platform with the use of electrochemical biosensors [26-28]. One label-free biosensor had TLS11a immobilized onto gold electrode surfaces and was incubated with multiple cell lines then coated with secondary TLS11a to form a sandwich structure like platform [28]. This biosensor was found to capture the human hepatocellular carcinoma line, HepG2, with a detection limit of 2 cells/mL, far below other previously reported cancer biosensor detection limits [28]. When incubated with the controls, colon, breast and prostate carcinoma, the biosensor was shown to be highly selective for HepG2 cells with very little or no binding to the controls [28]. This research suggests that not only was TLS11a effectively able to act as an HCC-probe in a biosensor platform exhibiting high specificity and high affinity to human HCC cells but also indicates the potential use in diagnostic applications.

While TLS11a has captured the attention of researchers, it is still unknown what epitope TLS11a recognizes and binds to on HCC cells. Recent research within the Weigum lab has explored TLS11a binding and localization studies. Through fluorescent confocal microscopy of MEAR cells labeled with TLS11a/Alexa-546, membrane and lysosome/endosome dyes, experiments showed aptamer binding to the membrane of MEAR cells and internalization and localization to endosomal or lysosomal compartments [29]. Western blot studies also suggest that TLS11a binds to a cell surface protein with a 21 kDa aptamer labeled protein band being present in all cell fractions excluding the hydrophobic membrane protein fractions; however, further studies are needed for a more conclusive result [29]. In conjunction of both the Weigum and Betancourt labs, TLS11a has also shown promising results for use as a targeted drug delivery system *in vitro*. Four different treatment groups were tested which included

TLS11a-functionalized nanoparticles loaded with the chemotherapeutic drug doxorubicin, blank nanoparticles loaded with doxorubicin, blank nanoparticles without doxorubicin and free doxorubicin [30]. After performing an MTT assay, it was determined that TLS11a-fuctionalized polymer nanoparticles exhibit the highest cytotoxicity when compared to the other nanoparticle treatment groups, exhibiting cell viabilities of less than 50% to 10% at the lowest and highest doxorubicin concentrations examined [30]. Free doxorubicin showed relatively similar cytotoxic effect as TLS11a-functionalized nanoparticles; however, for *in vitro* studies it is not uncommon for free doxorubicin controls to express such results due to the ease of its ability to penetrate the cell membrane and deliver effects compared to that of nanoparticle packaged doxorubicin which must be taken into cells via endocytosis [30]. This research demonstrates the potential TLS11a has for future use as a HCC-specific therapeutic treatment.

Collectively, these studies indicate that TLS11a demonstrates high specificity towards both mouse and human HCC cells, as opposed to normal liver and various cancer types, by its ability to selectively bind HCC cells and evoke cellular uptake. TLS11a has the potential to be used in both diagnostic and therapeutic applications.

1.6. Tissue Microarrays and Immunohistochemistry

Tissue microarrays are slides containing many individual tissues [31]. TMAs are created by sectioning cylindrical tissue core biopsies from frozen or paraffin blocks and fixing them on a slide with a defined grid [31, 32]. This allows for hundreds to thousands of samples to be compiled onto one slide for rapid analysis of all tissues and allows for better utilization of archived specimens [33]. Advantages of using TMAs are that one can prepare many tissue cores under the same conditions and analyze them together,

providing the opportunity to compare many samples simultaneously [33]. Purchasing TMAs can be more cost-efficient than purchasing individual samples and having to prepare them individually, thus saving time and supplies [33]. TMAs have been helpful towards identifying biomarkers and viewing morphological changes in tissue structure [33, 34]. Still, as with any new development, the usability of TMAs has been disputed and their applications are often trial-and-error. Some of these issues include tissue heterogeneity, whether selected sections are representative of the whole sample, tissue loss and concerns with fixation and embedding methods that have been shown to alter or destroy antigens [33]. Despite this, there are ways to resolve many of these problems and the utilization of TMAs is becoming more common in many applications.

One common application that TMAs are used in is immunohistochemistry studies. IHC is a method that is used to visibly identify antigens within tissue sections using specific targeting agents such as antibodies or aptamers [35]. These visual identifiers can be fluorophores or chromogenic labels which can be seen and imaged with fluorescence or light microscopy [36]. IHC studies are important for aiding in diagnostic and therapeutic applications and has become a powerful tool in helping scientist discover new disease biomarkers.

As previously mentioned, the HCC specific aptamer, TLS11a, is known to effectively discriminate HCC from normal liver tissue in mouse cells *in vitro* and biosensor applications. Unfortunately, very few studies have explored whether TLS11a is adequate for the use of HCC detection in humans [26, 27, 30]. Due to its high specificity towards HCC of mouse cells *in vitro,* TLS11a has the potential to be an important human HCC biomarker that needs to be further investigated.

1.7. Thesis Overview

The research presented in this thesis focuses on specificity of the TLS11a aptamer toward HCC and other malignancies. Specifically, using TMAs and performing IHC staining with TLS11a, I was able to address three key questions: (i) what human tissues does TLS11a bind (ii) is there a difference in TLS11a binding of normal vs. HCC liver and (iii) is binding correlated with tumor grade? Answering these questions may ultimately facilitate the discovery of an important human HCC biomarker that is recognized by the TLS11a aptamer. If so, TLS11a could have the potential to be used for various functions such as attachment to radioactive or magnetic particles for diagnostic purposes or conjugation to drug delivery vehicles for use as a targeting agent in future applications.

2. MATERIALS AND METHODS

2.1. Aptamer Sequences

Both HCC-specific aptamer, TLS11a, and control aptamer, TD4R, sequences listed in Table 1, were purchased from Integrated DNA Technologies (IDT; Coralville, Iowa) with either a fluorophore conjugation or biotinylation. TLS11a/AlexaFluor-546 and TD4R/AlexaFluor-546 was attached to an Alexa-Fluor®546 fluorophore (555 nm excitation/571 nm emission maxima) at the 5' terminal end through an amino group modification while TLS11a/fluorescein had a 5' primary amine modification with a fluorescein fluorophore (495 nm excitation/520 nm emission maxima) attached to an internal thymine residue closest to the 3' end. Lastly, biotinylated TLS11a had a 5' biotin modification. Both TLS11a and TD4R consisted of 63 nucleotides and all aptamers had similar melting temperatures, 71.9 °C and 73.2 °C respectively and GC content as determined using IDT OligoAnalyzer 3.1 software (data not shown).

Table 1. TLS11a and control aptamers sequence information.

Aptamer	Target	Length	Sequence	Modification
TLS11a	Hepatocellular carcinoma	63 nucleotides	5' – ACA GCA TCC CCA TGT GAA CAA TCG CAT TGT GAT TGT TAC GGT TTC CGC CTC ATG GAC GTG CTG – 3'	AlexaFluor-546, Fluorescein or biotinylated
TD4R	Negative Control	63 nucleotides	5'– ATC CGT CAC ACC TGC TCT TGA CAC GCG TAC GGG TCC GGA CAT GTC ATA ACG GAC TGG TGT TGG – 3'	AlexaFluor-546

2.2. Tissue Microarrays

The TMAs utilized for this research were either formalin-fixed paraffin-embedded or fresh frozen tissues. Three different types of FFPE TMAs were purchased

from Protein Biotechnologies, Inc. (Ramona, California) and two types of FF TMA were purchased from US Biomax, Inc. (Rockville, Maryland). Specific details for these microarrays are listed in Table 2. Fresh frozen arrays, after excision, were frozen in liquid nitrogen, embedded in optimal cutting temperature compound (OCT) and fixed with cold acetone. Both FFPE and FF arrays, composed of human tissue and cytokeratin confirmed, were stored at 4°C upon arrival in our lab where they remained until being used, typically within 1-2 months. FFPE tissue core diameters ranged from 1.5 mm to 2 mm and a thickness of 4 µm while FF tissue cores had a 2-mm diameter and 5-8 µm thickness. Each array was supplied by the manufacturer with information about the tissue donors' sex, age and malignancy grade.

Table 2. FFPE and FF TMA information.

Formalin fixed paraffin embedded TMAs				
TMA	**Cases**	**Cores**	**Tissue type**	**Purpose**
1201 Multi-cancer array	12	24	Brain, breast, colon, liver, lung, prostate, and tonsil (normal and malignant cases)	Identify what tissue TLS11a binds
1426 Liver matched HCC array	16	48	Uninvolved liver with patients matched HCC	Determine if TLS11a can differentiate between normal and HCC tissue
1427 Graded liver cancer array	48	96	Multiple diseased liver states	Determine if TLS11a binding is correlated with tumor stage
Fresh frozen TMAs				
TMA	**Cases**	**Cores**	**Tissue type**	**Purpose**
FMC282a Multi-organ cancer array	28	28	Breast, colon, esophagus, kidney, liver, lung, ovary, rectum, skeletal muscle, skin, stomach, testis, thyroid gland and vulva (normal and malignant)	Identify what tissue TLS11a binds
FLV402 Graded liver matched HCC	20	40	Uninvolved liver (cirrhosis) with matched HCC	Determine if TLS11a can differentiate between normal and HCC tissue and if binding is correlated with tumor grade

2.3. Paraffin Removal and Rehydration

TMAs were first deparaffinized with three sequential immersions in fresh xylene (5377, Avantor Performance Material, Inc.; Center Valley, Pennsylvania) for 10 minutes each. Slides were then rehydrated with decreasing concentrations of ethanol (100%, 95%, and 70%) for 5 minutes each and rinsed for 5 minutes with Dulbecco's phosphate buffered saline (PBS; BupH Dry Buffer Pack #28374, Pierce/Thermo Scientific™).

2.4. Antigen Retrieval

After paraffin removal and rehydration, select TMAs were subject to heat-induced epitope retrieval with Tris-EDTA buffer or sodium citrate buffer. Tris-EDTA, pH 9, was made with Tris base (BP152-1, Fisher Scientific) and ethylenediaminetetraacetic acid (EDTA; E9884, Sigma-Aldrich) while sodium citrate buffer, pH 6, was made with tri-sodium citrate (S4641, Sigma-Aldrich). Both solutions were mixed with Tween® 20 (P5927, Sigma-Aldrich) to reduce non-specific binding. Beakers were filled with enough buffer solution to cover the slides, placed on a hot plate, and allowed to reach 98°C. Slides were then immersed into the buffer solution, and the beaker was covered with foil, incubated for 20 minutes while ensuring the temperature of the buffer solution remained at a steady 98°C. Once incubation was complete, the beaker was removed from the hot plate and allowed to cool for 20 minutes at room temperature. Lastly, the slides were rinsed with PBS and were then available for the protocol to proceed with blocking.

2.5. Aptamer Refolding

If aptamer refolding was performed prior to staining, the aptamer was diluted in PBS containing 5 mM $MgCl_2$ and allowed to heat at 95°C for 10 minutes. After removal from heat, the aptamer was cooled to room temperature overnight.

2.6. Primary Fluorescent Staining and Mounting

To reduce non-specific binding, slides were incubated with a blocking buffer of 1% bovine serum albumin (BSA; A3059, Sigma-Aldrich) and 0.1 mg/mL tRNA (R5636, Sigma-Aldrich) in PBS for 1 hour. Slides were then incubated with PBSA wash buffer (0.1% BSA in PBS) and incubated with aptamer, TLS11a or TD4R, in PBSA overnight at 4°C. Next, slides were washed two times with PBSA for 5 minutes each then incubated with 1 drop of NucBlue® Live Cell Stain (R37605; Molecular Probes® Life Technologies; 347 nm excitation/483 nm emission maxima) in PBSA, for 15 minutes at room temperature, and again rinsed with PBSA. Slides were then mounted with either 90% glycerol (G9012, Sigma-Aldrich) or Prolong® gold antifade (P36934, Molecular Probes® Life Technologies) for imaging. Primary staining methods and incubation times remained constant for all assays unless stated otherwise. Negative controls were performed under identical conditions with the aptamer being replaced with PBSA.

2.7. Indirect Staining

For assays that were imaged at NIR wavelengths, a secondary antibody was used as an indirect staining method. Following paraffin removal and antigen retrieval, slides were incubated with blocking buffer for 30 minutes and labeled with 100 nM TLS11a/Fluorescein overnight at 4°C. Next, the slides were washed three times with PBSA, 5 minutes each, and incubated with 1 μg/mL of mouse monoclonal anti-fluorescein antibody (6A4; ab6213, Abcam) in PBSA, for 2 hours, at room temperature. Again, slides were washed three times, 5 minutes each, followed by incubation with 5 μg/mL goat anti-mouse/Alexa-fluor®750 secondary antibody (A21037, Invitrogen™/Thermo Fisher Scientific) for 1 hour at room temperature, followed by three

subsequent PBSA washes for 5 minutes each. Lastly, the slides were incubated with 1 drop NucBlue® Live Cell Stain in PBSA for 15 minutes, washed and mounted with Prolong® gold antifade.

2.8. Colorimetric TMA Staining and Mounting

For slides undergoing colorimetric staining, following paraffin removal and rehydration, slides were incubated for 10 minutes in 3% hydrogen peroxide (H_2O_2; 216763, Sigma-Aldrich) in methanol (A4081, Fisher Scientific) to quench endogenous peroxidases. Slides were then washed twice with cold PBS, 10 minutes each, and blocked with blocking buffer for 1 hour at room temperature. Slides were then subject to blocking of biotin using 0.1 mg/mL neutravidin (31000, Thermo Fisher Scientific) in PBSA, for 15 minutes, followed by three 10 minute washes with PBSA. To block any additional binding sites on the neutravidin molecule, the slides were incubated with 0.5 mg/mL biotin (B4501, Sigma-Aldrich) in PBSA for 1 hour and again washed three times with PBSA. One slide was then incubated with a 100 nM solution of biotinylated TLS11a in PBSA while the negative control was incubated with PBSA only, overnight at 4°C. To remove any unbound aptamer, slides were washed three times with PBSA, 5 minutes each, and incubated with 1 mg/mL streptavidin-HRP (A2664, Invitrogen™/Thermo Fisher Scientific) in PBSA for 30 minutes at room temperature. After washing, the reactions were visualized by incubating the slides with diaminobenzidine substrate kit 10x (DAB; 882014, Pierce/Thermo Scientific) for 5 minutes and followed with two PBSA washes for 5 minutes each. For visualization of the nuclei, slides were counterstained with modified Mayer's hematoxylin (72804, Richard-Allen Scientific™/Thermo Scientific), for 5 minutes, rinsed and mounted with glycerol.

2.9. Frozen TMA Staining

Frozen tissue arrays were fixed for 8 minutes at -20°C in pre-cooled acetone and sequentially washed four times, 5 minutes each, with wash buffer (PBS with 4.5 g/L glucose and 5 mM $MgCl_2$). Slides were incubated with blocking buffer, prepared by adding 20% fetal bovine serum (FBS), 0.1 mg/mL yeast tRNA and 1 mg/mL BSA into wash buffer, for 30 minutes at room temperature. Slides were rinsed and incubated with 100 nM TLS11a/AlexaFluor-546 at 4°C overnight. Following two 5-minute washes, slides were incubated with 1 drop NucBlue® Live Cell Stain in PBSA for 15 minutes and followed up with two PBS rinses. Lastly, slides were mounted with Prolong® gold antifade and allowed to dry overnight. Negative controls were performed under identical conditions except for PBSA being used in place of TLS11a during the overnight incubation period.

2.10. Imaging

All tissues stained with fluorescent probes stained slides were imaged within 1 week of mounting. EVOS® FL Auto Imaging System (Life Technologies), an inverted multi-channel fluorescence and transmitted light imaging system was used for TMA imaging. A DAPI LED light cube (357/44 nm excitation; 447/60 nm emission) was used for imaging the NucBlue stained nuclei of cells, while the RFP (531/40 nm excitation; 593/40 nm emission), GFP (470/22 nm excitation; 510/42 nm emission) and CY7 (710/40 nm excitation; 775/46 nm emission) LED light cubes were used for imaging AlexaFluor-546, fluorescein and goat anti-mouse/AlexaFluor-750 labeled aptamers, respectively. Imaging for colorimetric stained arrays was done under transmitted light microscopy. For both fluorescence and transmitted light microscopy, scans and images

were obtained from each tissue core. For whole tissue core scans, the individual micrographs were stitched together using the EVOS FL Auto software. Scans were performed of each whole tissue core using either a 10x (NA 0.40, Olympus) or 20x objective lens. For images, multiple fields of view per tissue core were acquired using either a 20x (NA 0.75, Olympus) or 40x (NA 0.65, Olympus) long working distance objective lens. The resulting pseudo-colored gray scale images were saved as both a composite and as individual channel, 8-bit or 16-bit, TIFF image files. All light, exposure and gain setting were identical for arrays under comparison. The saved images were imported to ImageJ, open source software from the National Institute of Health, for processing and fluorescence pixel intensity (grey level) quantification. Prior to taking any measurements, background noise was measured and subtracted in each image to correct for differences in the microscope acquisition. The mean fluorescence intensity was collected for arrays containing multiple tissue types while integrated intensity (mean * area) values were collected from arrays limited to liver tissue. When calculating the mean fluorescence intensity (arbitrary units) of tissue core scans, multiple regions of interest (ROIs) were used to obtain the collective mean fluorescence intensity of the tissue (Appendix, Figure A1). The same ROIs were used throughout the array and for comparison arrays. When determining the fluorescence intensity of images, all measurements were limited to a histogram determined stack threshold (Appendix, Figure A2). The integrated intensity, also limited to a stack threshold, was used for arrays made up of liver tissue alone. This allowed for a more detailed analysis, as the means tended to be similar throughout, and this value considered differences in the threshold area. Multiple fields of view were used to account for variability throughout the tissue and

assess the overall tissue core. For better visual representation, false-colored images that have been adjusted for brightness and contrast are used throughout this thesis.

2.11. Statistical Analysis

Fluorescence quantitative data is expressed as mean ± standard deviation or integrated intensity ± standard deviation. Ratios (HCC/uninvolved liver) were obtained in some instances to determine if there was an increase of aptamer binding between certain assays. All quantitative fluorescence statistical analysis was performed using SigmaPlot Software 12.5 (IBE, Armonk, NY, USA). To analyze the significant difference between two groups, an unpaired Student's t-test was performed and when comparing more than three groups, a one-way ANOVA was used followed by a LSD post hoc test. For all statistical tests, values of $p<0.05$ were considered statistically significant.

For analysis of images acquired with transmitted light microscopy, IHC Profiler, an Image J plugin, was used to determine if staining would be considered positive or negative [37]. Using IHC Profiler, images underwent deconvolution and the resulting DAB images staining intensity was analyzed (Appendix, Figure A3). The image scoring was achieved by classifying an 8-bit (0 to 256 pixels) image pixel intensity into categories of high positive (0 to 60 pixel values), positive (61 to 120 pixel values), low positive (121 to 180 pixel values) and negative (181 to 235 pixel values) while any pixels above 235 are not considered as they generally represent tissues high in fat or areas that are blank [37].

3. RESULTS AND DISCUSSION

3.1. Optimization of TLS11a Concentration for Labeling

Formalin-fixed paraffin-embedded multi-tissue arrays (TMA-1201) were subjected to a 30-minute blocking period and incubated with a 50 nM, 100 nM or 200 nM concentration of TLS11a/AlexaFluor-546 for 2 hours at room temperature. TMAs were mounted with 90% glycerol and compared to determine the optimal working concentration of TLS11a. After image collection, images acquired using the 40x objective were used to measure the overall mean pixel intensity of HCC tissue for each concentration (Figure 2A). A one-way ANOVA followed by Holm-Sidak post hoc test to revealed HCC stained with 100 nM TLS11a had a significantly higher fluorescence intensity ($p < 0.001$) than HCC tissue stained with 50 nM or 200 nM TLS11a (Figure 2B). As a result, 100 nM TLS11a was chosen as the optimal working concentration for future experiments.

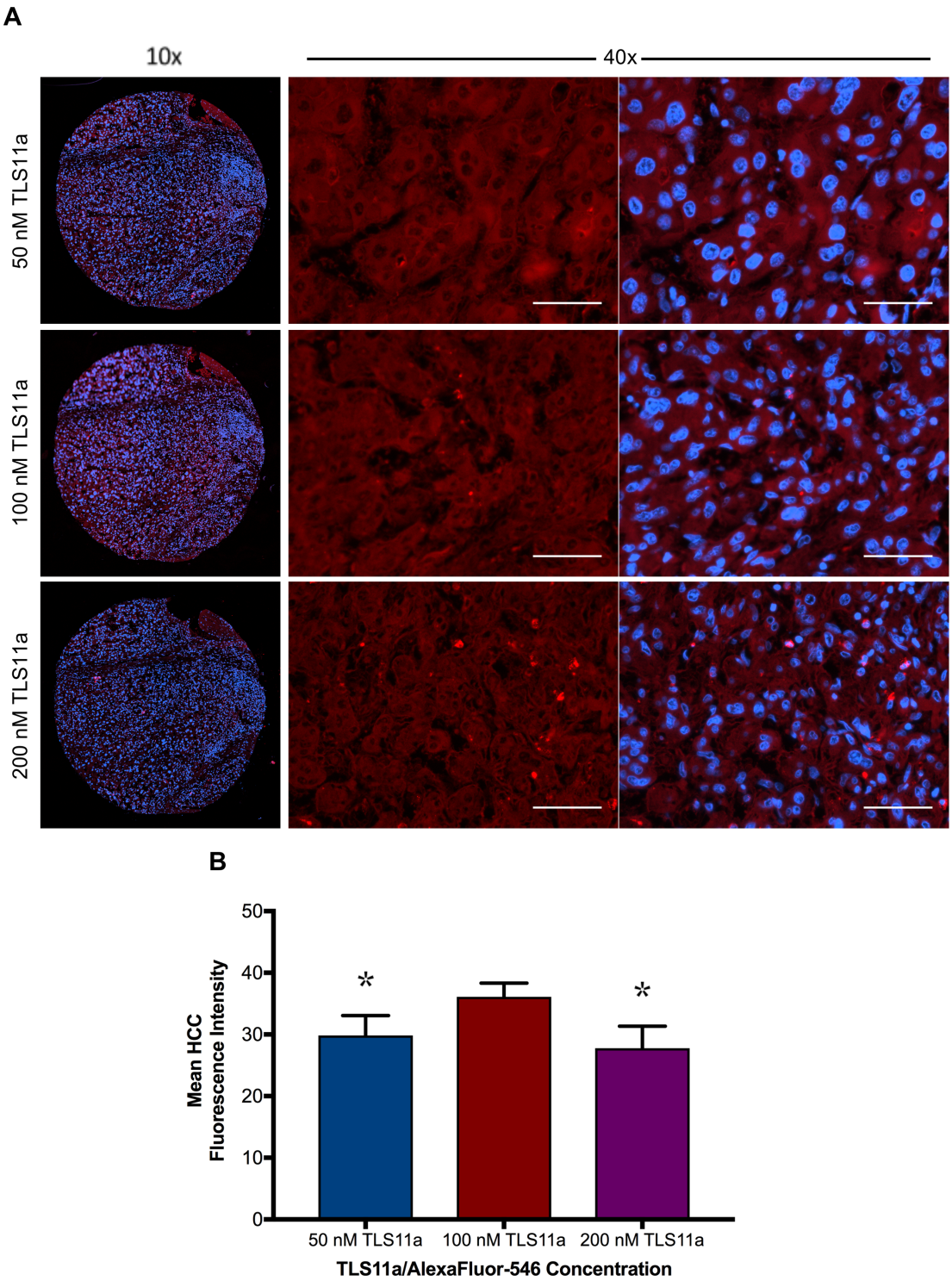

Figure 2. Fluorescence images of TLS11a concentration optimization on human HCC tissue. (A) HCC tissue cores labeled with 50 nM, 100 nM and 200 nM TLS11a/AlexaFluor-546 (red) with NucBlue stained cell nuclei (blue) scanned at 10x magnification (left). HCC tissue cores corresponding 40x magnified view from the red channel only (center) and merged red/blue channel (right). Scale bar represents 50 µm. (B) Quantitative analysis showing the mean fluorescence pixel intensities (arbitrary units). For comparative analysis, each array's HCC tissues 40x images were measured. $p<0.050$ considered to be significant.

To investigate aptamer binding to other tissue types, including normal tissues from liver, breast, brain, and lung among others, the full 100 nM TLS11a labeled array was analyzed. The mean fluorescence intensity of each normal tissue type was collected, using the same methods previously stated, and compared to the mean fluorescence intensity of HCC tissue (Figure 3A). A higher pixel intensity indicates more fluorescence and is thus representative of aptamer binding. Results from a one-way ANOVA indicate that TLS11a binding was significantly higher in HCC tissue than any other normal tissue type (Figure 3B), including normal liver tissue ($p < 0.001$). A moderate amount of labeling was seen in normal liver and cerebral cortex tissue; however, it was not significant when compared to that of HCC. These results support the idea that TLS11a not only shows high specificity to HCC but also that it can differentiate between normal liver and HCC.

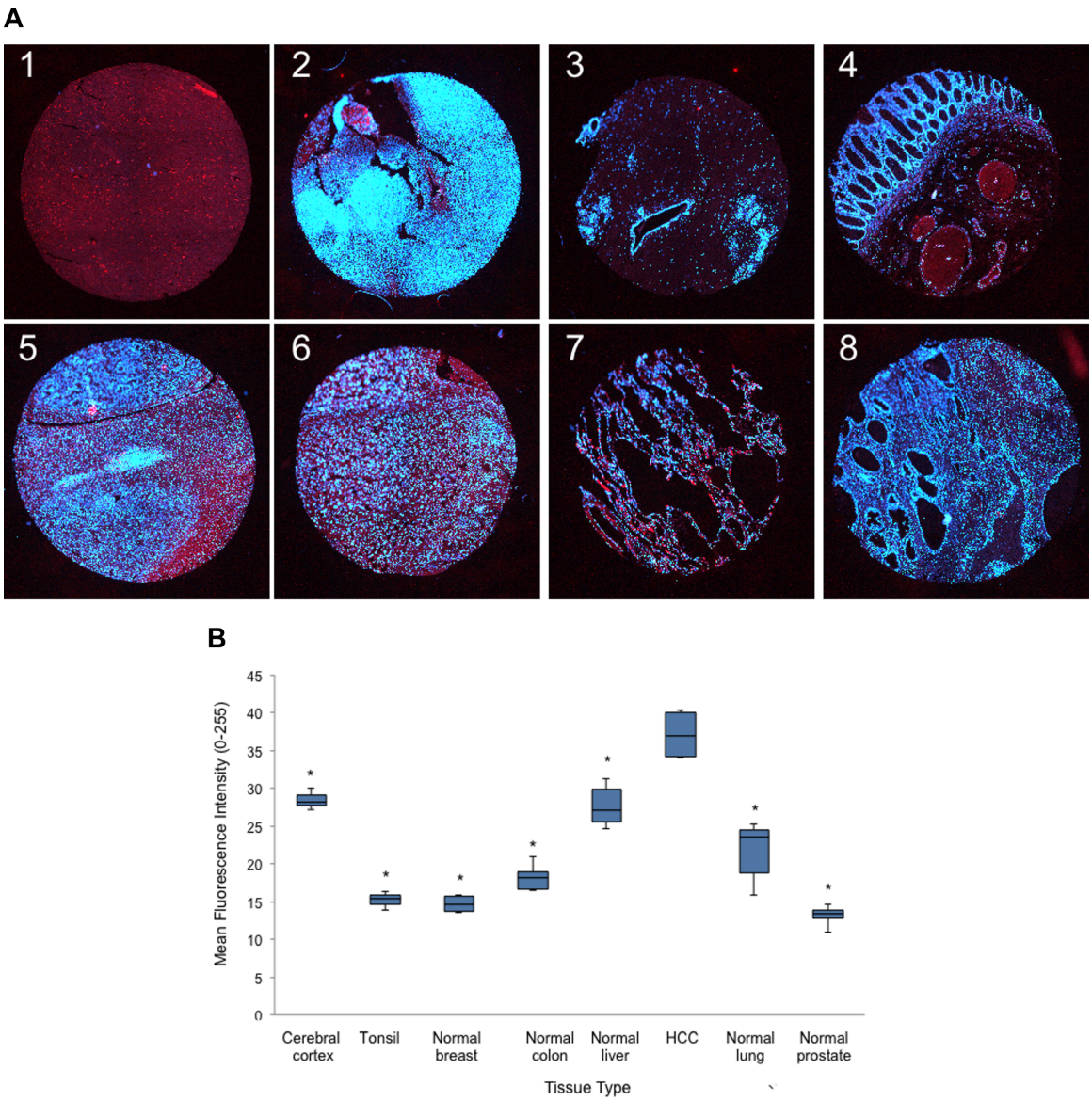

Figure 3. 100 nM TLS11a/Alexa-Fluor-546 stained TMA fluorescence images and quantification. (A) 10x scanned TMA cores merged fluorescence images of different tissue types (1) Cerebral cortex (2) Tonsil (3) Normal breast (4) Normal colon (5) Normal liver (6) HCC (7) Normal lung (8) Normal prostate. Hoescht nuclei stain (blue) and TLS11a/AlexaFluor-546 (red). (B) Red channel fluorescence pixel quantification of TLS11a/AlexaFluor-546 (n=6) using the same method as previously stated. $p<0.050$ considered to be significant by one-way ANOVA followed by Holm-Sidak post hoc test.

3.2. Aptamer Refolding

Aptamers secondary structure is important for epitope binding. Temperature change and ion concentration cause changes in the system thus altering the folding of the

aptamer. If folded improperly, the aptamer is less likely to recognize and interact with the target epitope resulting in a decreased binding efficiency [38]. Figure 4 shows the predicted secondary structure of TLS11a using IDT's OligoAnalyzer 3.1 software. The resulting ΔG of -27.11 indicated aptamer stability under experimental conditions of 4°C and 5 mM $MgCl_2$.

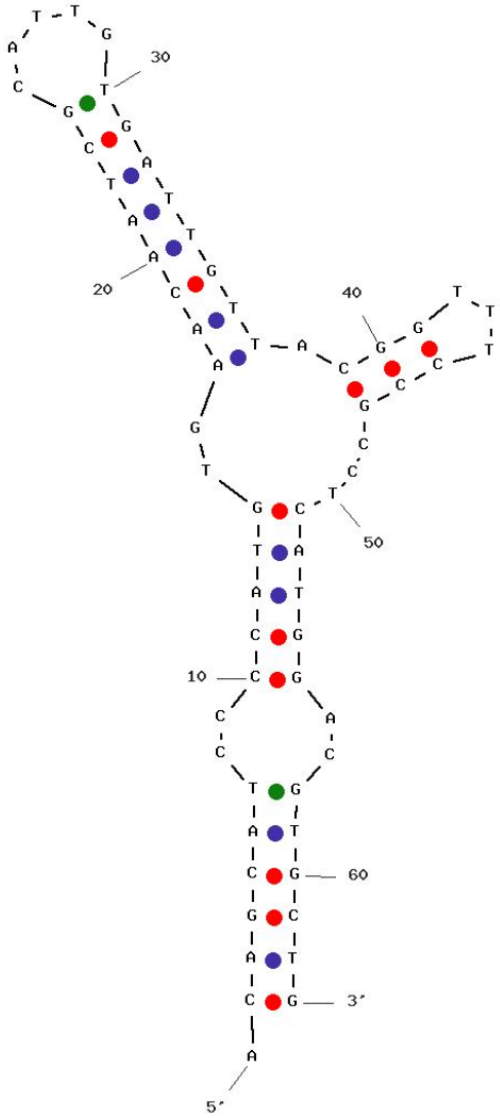

Figure 4. TLS11a secondary structure. Generated using IDT's OligoAnalyzer 3.1 software under experimental conditions. ΔG= -27.11 kcal·mole^{-1}.

To ensure proper folding, an assay was performed using matched liver 1426 TMAs with TLS11a/Fluorescein. One array was treated with TLS11a that had first undergone refolding while the control was treated without TLS11a refolding. Figure 5A shows the same tissue cores from both treatments. A common threshold was set and quantitative analysis was performed using whole core scans. The mean pixel intensity was found to be unhelpful as most HCC tissue demonstrated similar means and most uninvolved tissue had the same means. As a result, the mean integrated intensity (mean * area) was used to eliminate blank areas caused by differences in tissue sectioning and gave more conclusive information. First, the integrated intensity values of each uninvolved liver tissue (n=16) and HCC tissue (n=30) were used to determine if the aptamer could differentiate between normal and HCC tissue (Figure 5B). An unpaired two-tailed Student's t-test determined there was no significant difference between the integrated intensity of uninvolved liver and HCC tissue for either the aptamer refolding ($p=0.9678$) or no aptamer refolding array ($p=0.9667$). This indicated there was not a large difference of aptamer binding to HCC tissue as compared to uninvolved liver tissue. In the few instances there appeared to be a difference, it occurred on both arrays suggesting it was due to differences in tissue heterogeneity rather than aptamer functionality. For further analysis, the ratio of each array was compared (Figure 5C). Using the same statistical test, no significant difference ($p=0.8206$) was found between the two treatments (n=30). Results indicate that aptamer refolding was not necessary for future assays, as it did not increase the aptamer's ability to bind. If aptamer refolding were necessary, I would have expected to see higher ratios from the aptamer refolding treatment relative to the no refolding control.

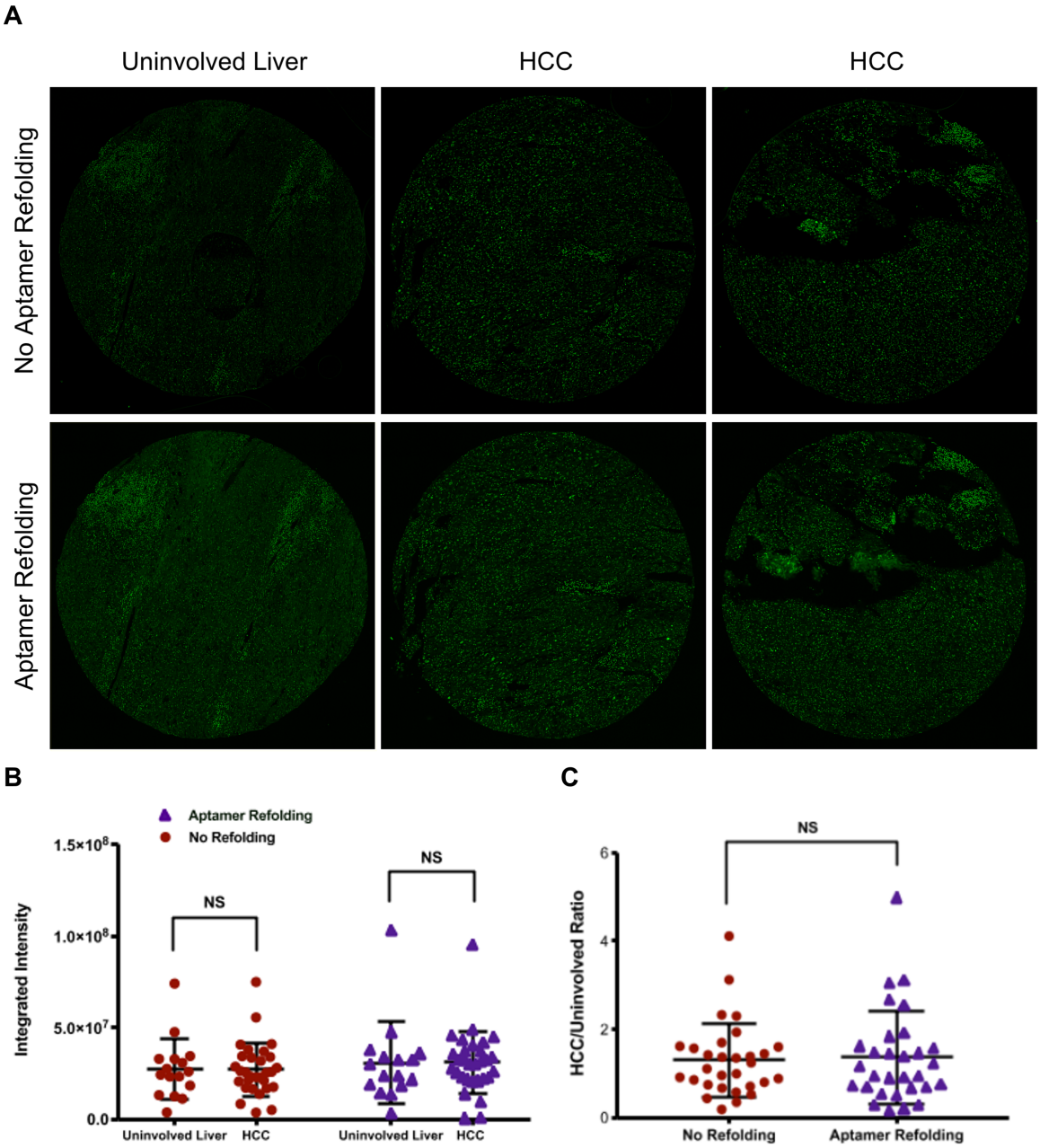

Figure 5. Aptamer folding assay. (A) GFP channels 20X scanned tissue cores showing the same case comparing the array without aptamer refolding and the array treated with aptamer refolding. Each case consisted of one uninvolved liver tissue core and two matched HCC tissue cores. (B) Quantitative analysis of the integrated intensity of each case uninvolved liver (n=16) and matched HCC tissues (n=30) of both the array without refolding (red) and array that had undergone aptamer refolding (purple). No significant difference was found between uninvolved liver and HCC tissue for either treatment. (C) Quantitative analysis using the HCC/uninvolved liver ratio (n=30) for both treatment groups. No significant difference was found for either treatment. Both graphs show dot plot of each core and horizontal lines indicate the mean ± standard deviation.

3.3. Antigen Retrieval

Formalin, a commonly used aldehyde-based fixative, is used to help to maintain tissue morphology and protect it from degradation. Formalin works by penetrating the tissue and reacting with primary amino acids, amides, thiols, hydroxyl and cyclic aromatic rings which ultimately results in cross-linking [39, 40]. Consequently, these changes in protein structure can cause a loss of antigenicity. This occurrence, also known as epitope masking, can result in the inability of antigens and antibodies to interact [39, 40]. Due to arrays being FFPE, antigen retrieval was performed in case epitope masking had occurred. Antigen retrieval is a method to help unmask antigens and restore proteins back to their original structure [39, 41]. Heat has been shown to be one of the most effective methods of antigen retrieval though there are many other approaches [39, 40].

To determine if antigen retrieval was necessary, and if so, which buffer was most beneficial, Tris-EDTA buffer pH 9, sodium citrate pH 6 and a control with no antigen retrieval were tested. All other experimental conditions were identical with a 2-hour aptamer incubation at room temperature. After imaging, intensity information of normal and HCC tissues was collected using ROIs from the grayscale 20x scans (Figure 6A). Ratios were obtained to determine which method demonstrated more TLS11a binding in HCC tissue compared to normal liver tissue. Thus, the greater ratio indicates more differentiation between HCC and normal tissue. Looking at ratios between no antigen retrieval (1.14) and antigen retrieval with sodium citrate (1.29) and Tris-EDTA (1.48), I determined that there was greater epitope retrieval when performing antigen retrieval with Tris-EDTA buffer pH 9 (Figure 6B) which was confirmed with a one one-way ANOVA ($p < 0.050$).

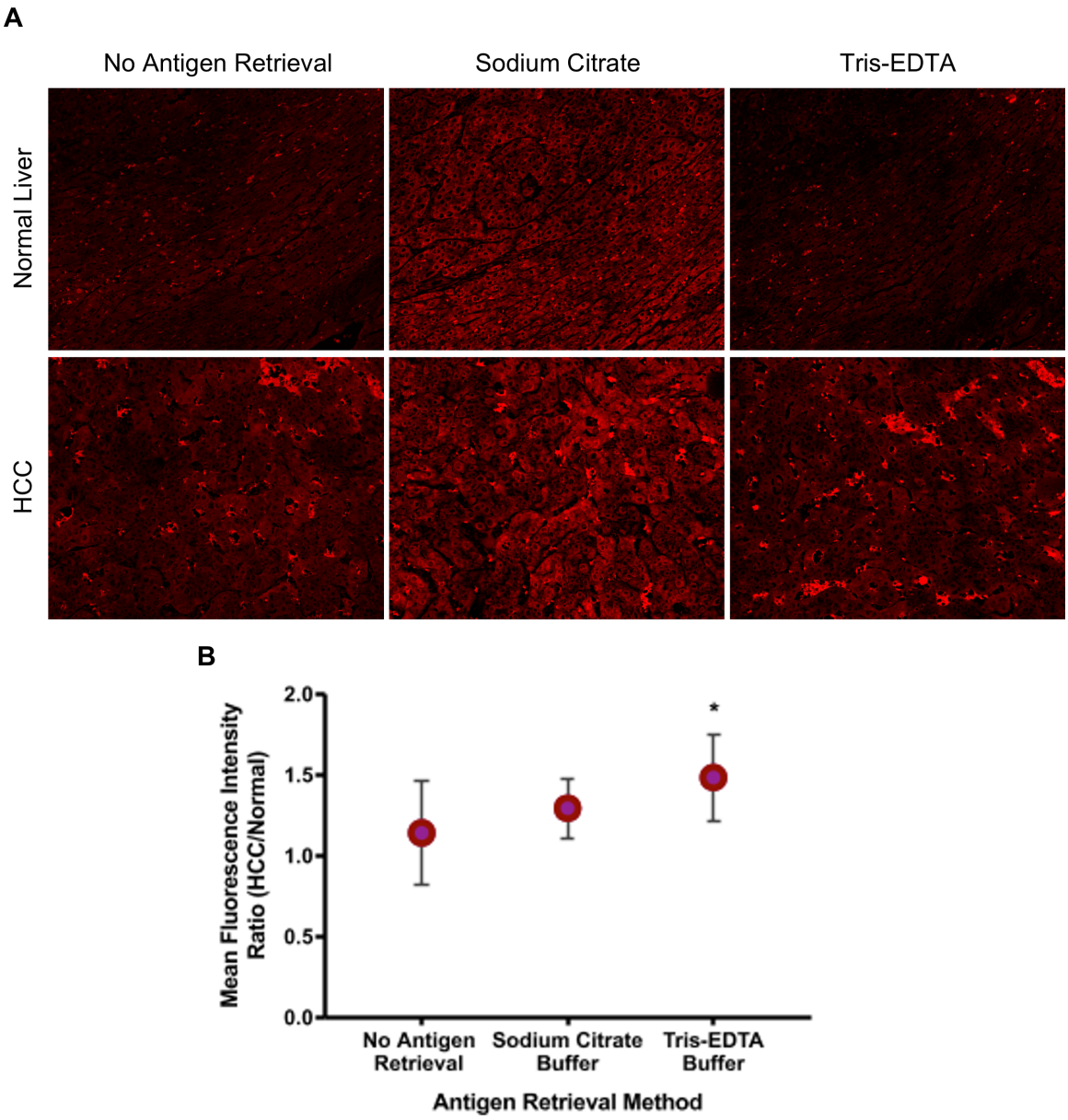

Figure 6. Antigen retrieval assay. (A) Fluorescence images collected with a 20x lens from the RFP channel showing the normal liver (top) and HCC tissue (bottom) with inset of red channel only (B) Quantitative data of mean fluorescence intensity ratio (HCC/normal). $p<0.050$ considered to be significant with one-way ANOVA followed by Holm-Sidak post hoc test using HCC/normal liver ratios (n=12).

3.4. Control Assays

Slides were blocked for 30 minutes and incubated with either 100 nM

TLS11a/AlexaFluor-546,100 nM TD4R/Alexafluor-546 or no aptamer (PBSA) for 2

hours at room temperature. Antigen retrieval was not used for this experiment. Using the red channels gray scale images obtained using a 40x lens, the mean integrated intensity was obtained and analyzed with a one-way ANOVA followed by Holm-Sidak post hoc test (Figure 7A).

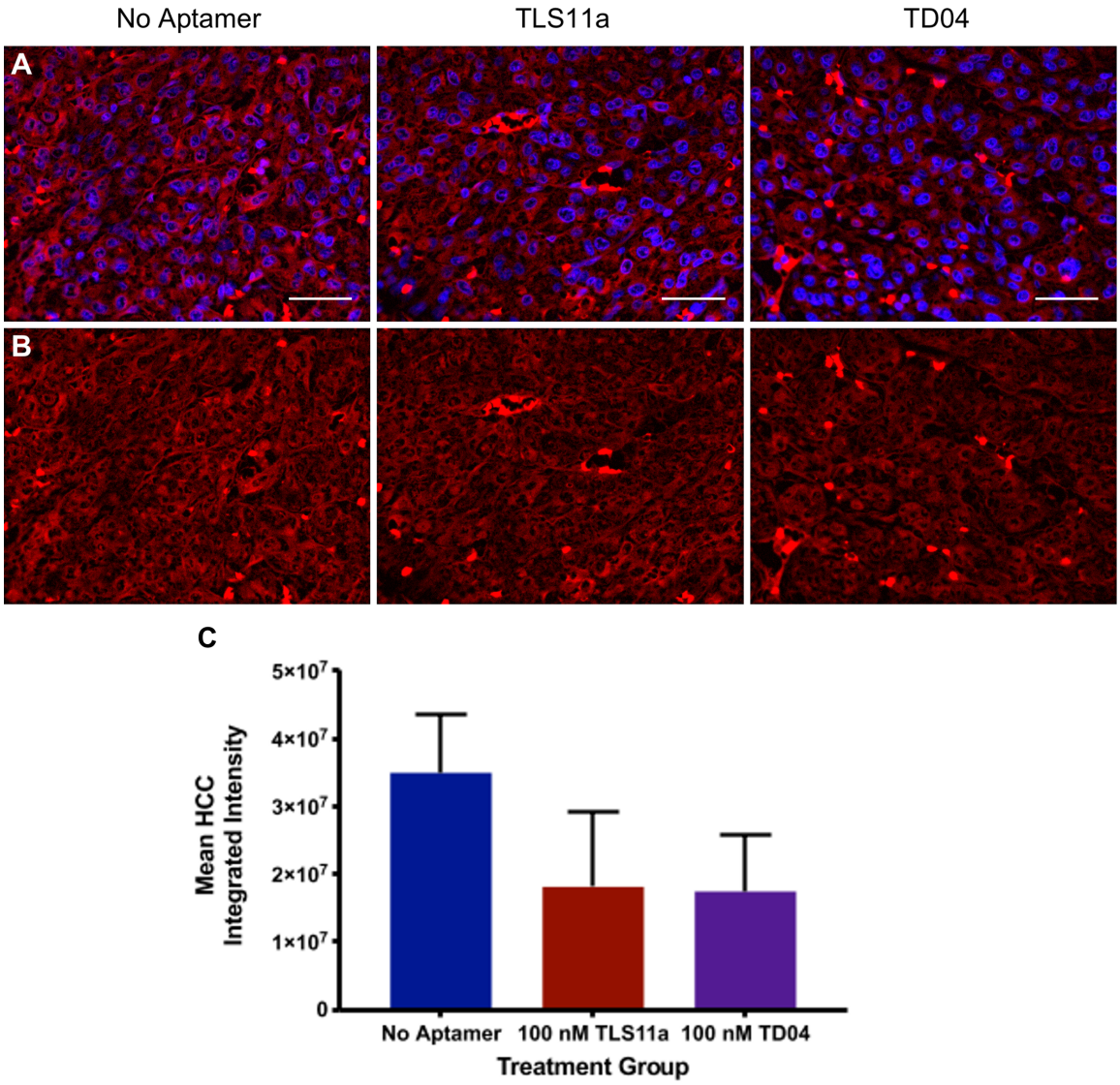

Figure 7. Control assay using 100 nM TLS11a/AlexaFluor-546, 100 nM TD4R and a negative control treatments. 40x fluorescence images show (A) merged NucBlue nuclei stain (blue) and TLS11a/AlexaFluor-546 (red) images and (B) Red channel images only of the negative control HCC tissue (left), 100 nM TLS11a/AlexaFluor-546 stained HCC tissue (center) and 100 nM TD4R stained HCC tissue (right). Scale bar represents 50 µm. (C) Quantitative data of the mean HCC integrated fluorescence intensity from 40x images compared using one-way ANOVA followed by Holm-Sidak post hoc test (n=4) showing no significant difference between the three groups.

It was expected that HCC tissue stained with TLS11a would exhibit the greatest integrated intensity and HCC tissues stained with TD4R or PBSA (negative control) would have very little to no signal. However, the negative control HCC tissue exhibited the highest mean integrated intensity (3.50E7 ± 8.53E6), followed by TLS11a/AlexaFluor-546 (1.81E7 ± 1.11E7) and TD4R/AlexaFluor-546 (1.75E7 ± 8.40E6). A one-way ANOVA indicated there was no statistical difference between the negative control and TLS11a treated HCC tissue ($p= 0.0801$) or TLS11a and TD4R HCC tissue ($p=0.9211$) (Figure 7B). These results suggest that there was no specific binding, a problem with the fluorescence probe, or issues with autofluorescence. It was hypothesized that using a different fluorophore that could be imaged in an alternate channel may help rule out the problem, if not alleviate the problem.

For this reason, a negative control and 100 nM TLS11a treatment was conducted using TLS11a/Fluorescein. Antigen retrieval with Tris-EDTA was performed and the incubation period was changed to overnight at 4°C. 20x scans and 20x images (Figure 8A-B) were collected from the GFP channel. 20x images, limited to a stack threshold, were used to collect integrated intensity measurements (Figure 8C). A two-tailed Student's t-test indicated there was not a significant difference ($p=0.4515$) between the negative control (1.88E6 ± 6.04E5) and aptamer stained array (4.18E6 ± 2.41E6).

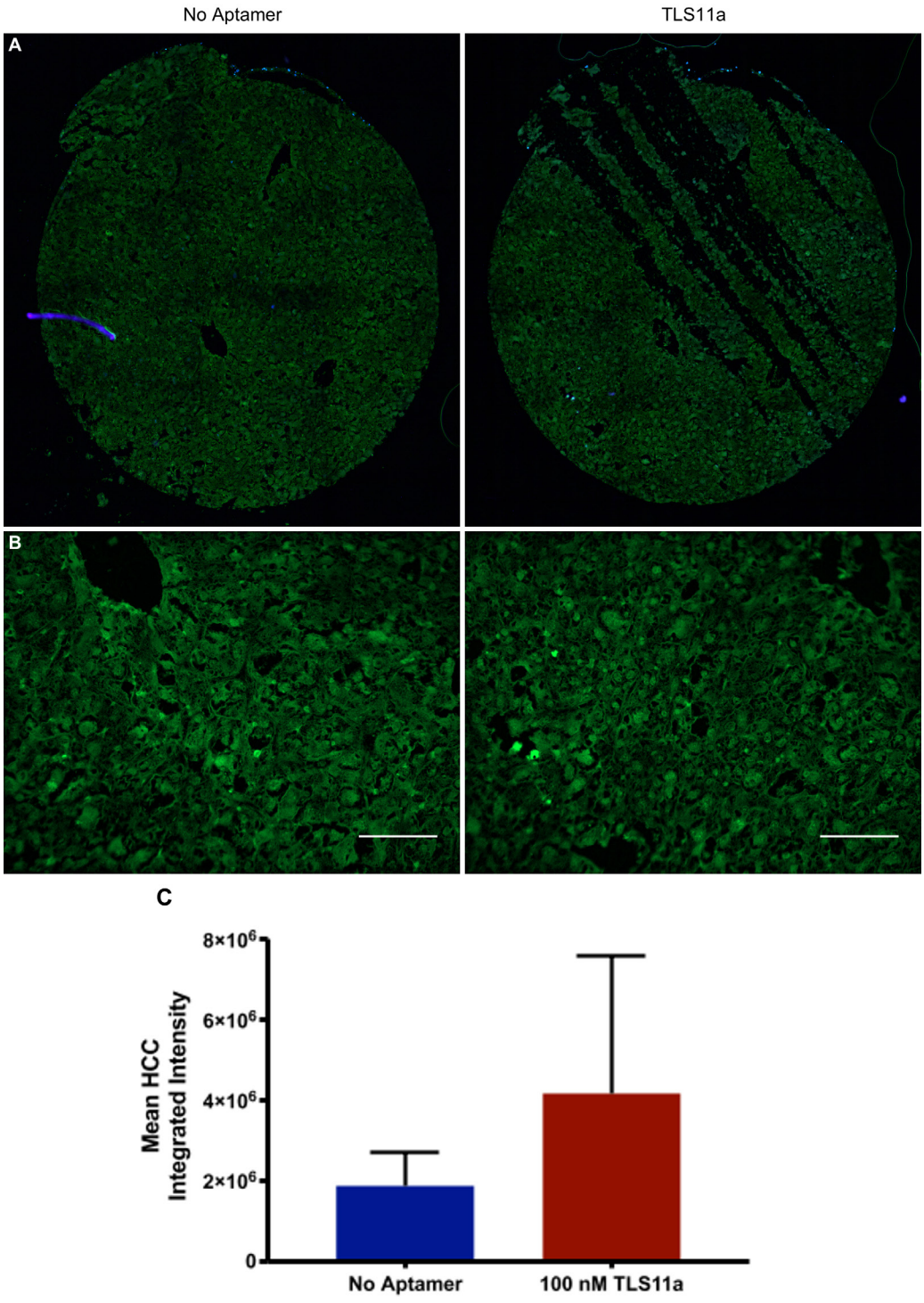

Figure 8. Control assay using negative control and 100 nM TLS11a/Fluorescein treatments. Fluorescence images show green channel (A) 20x scans and (B) 20x images of the negative control (left) and 100 nM TLS11a/Fluorescein (right) HCC tissue. Scale bar represents 100 μm. (C) Quantitative mean HCC integrated intensity information using 20x images, set to an identical threshold. $p<0.050$ was considered significant using a two-tailed Student's t-test (n=2).

Again, specific binding was not found, so other possible sources of error were explored. The next possibility was the fluorescence being quenched. One of the causes of fluorescence quenching is using high concentrations. If fluorophores are clustered together, self-quenching can occur through electron energy transfer. If the electron is absorbed by another molecule before reaching its ground state, it will cause the fluorescence to be quenched. Fluorescein intensity has been known to decrease when stored for long periods of time and when dissolved in aqueous solutions [42]. Fluorescein has also been known to suffer substantial quenching in environmental conditions below pH 7 and in the presence of amino acids tryptophan and tyrosine [42, 43]. However, Alexa dyes are known for being stable, even when used at high concentrations, and the probability of both fluorophores being quenched is highly improbable [42]. Furthermore, previous studies show significant fluorescence using both fluorophores on mouse HCC cells, indicating fluorophore quenching is not the problem (data not shown). The most likely possibility is that the fluorescence signal being seen is mostly autofluorescence from endogenous molecules or tissue fixation.

There are also many intrinsic biomolecules that absorb light acting as endogenous fluorophores [44]. Many fluorescence molecules are known to accumulate at extremely high levels in the liver (Table 3), the most common being lipofuscins, NADP-NAD(P)H, flavins, collagen and elastin [45, 46]. This accumulation is a consequence of the liver being highly metabolically active, thus producing large amounts of NAD(P)H and flavins for use in redox reactions, as well as having a high amount of collagen and elastin due to the liver having a large complex vasculature system [45]. Of the molecules, lipofuscins are most commonly found in lysosomes, NAD(P)H and flavins tend to accumulate in the

mitochondria and cytosol, while collagen and elastin make up the connective and stroma tissue [45]. Another source of AF is caused by formalin fixation when formaldehyde covalently crosslinks proteins, forming methylene bridges in tissues, producing fluorescent compounds [45]. After fixation, tissues are embedded in paraffin, and if not completely removed, paraffin can contribute to autofluorescence or cause poor staining.

Table 3. Sources of endogenous molecules that contribute to tissue autofluorescence.

Autofluorescence Source	Biological constituents	Excitation range (nm)	Emission range (nm)
Collagen	Extracellular fibrous proteins	330-410	470-520
Cytokeratins	Intracellular fibrous proteins	480-325	495-520
NAD(P)H	Coenzymes in redox reactions	340-500	440-500
Elastin	Extracellular fibrous proteins	350-420	420-520
Fatty acids	Accumulated lipids	330-350	470-480
Flavins	Coenzymes in redox reactions	350-520	480-560
Formaldehyde induced	Fixative-induced	355-435	420-470
Lipofuscins/lipopigments/ceroids	Miscellaneous (proteins, lipids, retinoids)	400-500	480-700
Porphyrin derivatives	Protein prosthetic group	405	630-700
Vitamin A	Retinols and carotenoids	370-380	490-510

Having found both control assays were unsuccessful and that endogenous molecules can create fluorescence that spans both fluorophores emission spectrum, the most likely cause of these problems was thought to be autofluorescence. Near-infrared (NIR) fluorophores, using wavelengths above 700 nm, have been used to reduce tissue AF. Tissues show their lowest fluorescent properties at wavelengths above 700, known as the “diagnostic window,” due to less light scatter [47-49]. As a result, it was determined the next step would be to use indirect staining with a secondary NIR fluorophore. It was thought NIR would escape the inherent autofluorescence spectrum and using indirect staining would amplify the fluorescence signal.

3.5. Indirect Staining

Antigen retrieval, blocking and incubation times were identical for three 1201 TMAs with the aptamer staining specifics listed on Table 4, negative (-) indicating it was not added and positive (+) indicating it was added. An indirect staining method was used with the primary antibody being TLS11a/fluorescein which could then be labeled with an anti-fluorescein mouse antibody, which binds the fluorescein molecules on TLS11a, and the secondary antibody being a goat anti-mouse antibody conjugated to AlexaFluor-750 for detection in the near-IR range.

Table 4. Indirect staining specifics for each treatment group.

TMA name	TLS11a/fluorescein	Anti-fluorescein	GAM/Alexa-Fluor®750
Autofluorescence/negative control	-	-	-
Non-specific staining control	-	+	+
Near-IR array	+	+	+

Imaging and scans were performed on each array in DAPI, GFP and CY7 fluorescence channels using the same microscope settings for each array. Each array's normal liver and HCC tissue cores were measured for mean integrated intensity using 20x images, set to a stack threshold, of the CY7 channel (Figure 9A-B). Quantitative analysis of HCC tissue was performed using a two-tailed Student's t-test between first the autofluorescence and TLS11a/secondaryAlexaFluor-750 array and then the TLS11a/secondaryAlexaFluor-750 and non-specific array (Figure 9C). Although there does seem to be a large decrease in autofluorescence, there was not a significant difference between the negative control and aptamer stained array ($p=0.0731$).

Furthermore, the non-specific staining control had a higher mean integrated intensity for both normal liver and HCC tissue but also showed no significant difference between itself and the aptamer stained array ($p=0.4164$). The non-specific staining control having a larger mean integrated intensity suggests that it may not be the aptamer fluorescence that is being measured; rather the secondary antibody may be binding to other non-specific antigens, resulting in an increased fluorescence signal. Non-specific staining is known to occur if using too high of a primary or secondary antibody concentration. Another cause of non-specific staining is the use of BSA used for blocking. BSA contains bovine IgG, which can be recognized by the secondary antibody, causing increased non-specific binding [50].

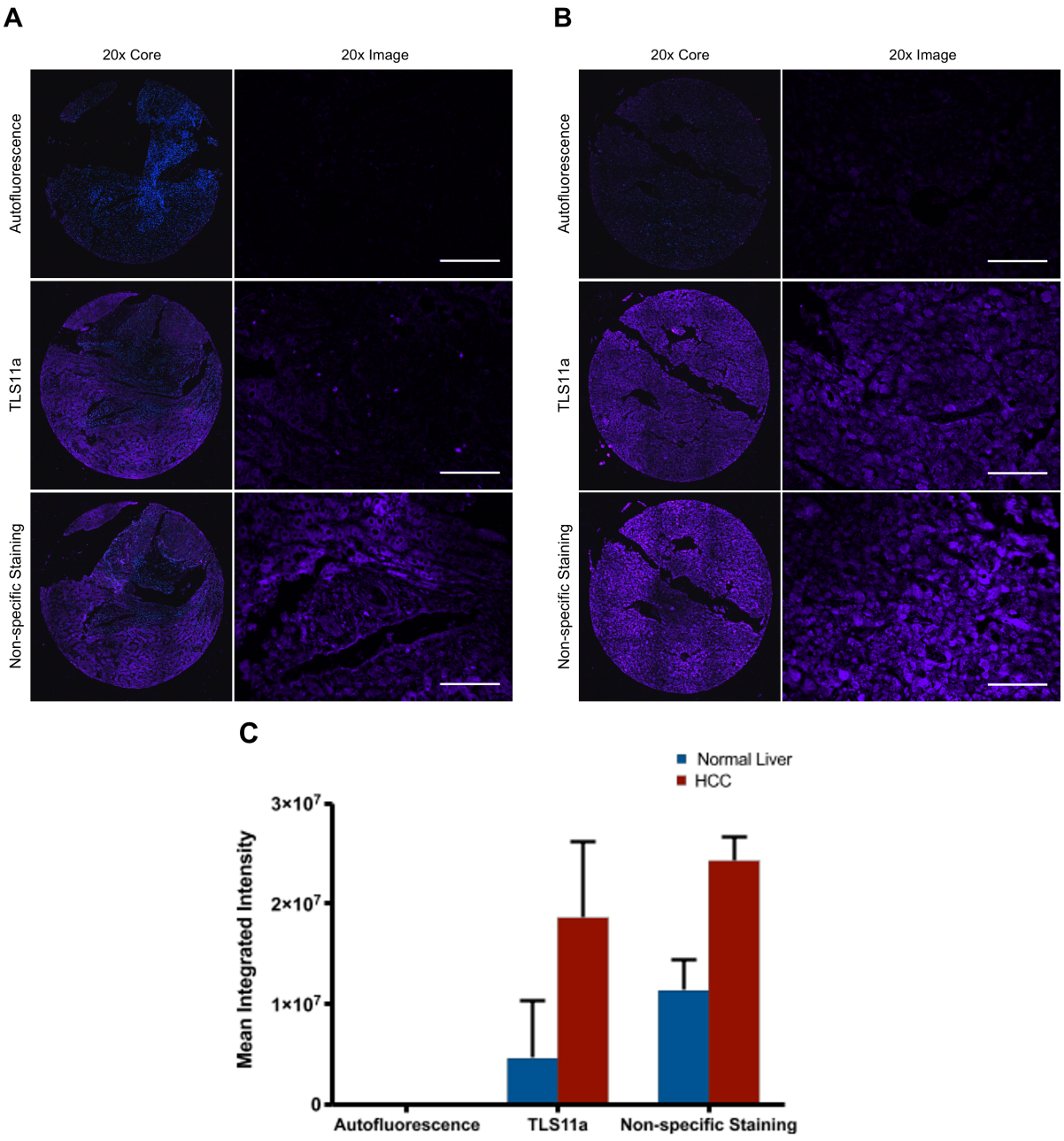

Figure 9. Indirect staining assay. Fluorescence images showing 20x scans (left) and 20x images (right) with Hoescht nuclei stain (blue) and TLS11a/secondary AlexaFluor-750 (purple). (A) Normal liver tissue of the autofluorescence TMA (top), TLS11a (middle) and non-specific stained array (bottom) (B) HCC tissue. Scale bar represents 100 μm. (C) Mean integrated intensity quantitative data. $p<0.050$ was considered specific with a two-tailed Student's t-test (n=2).

There was a noticeable drop of tissue autofluorescence when using a longer wavelength; however, there were large amounts of non-specific binding, further complicating things. There was also a decrease in fluorescence intensity from the DAPI channel which was rather interesting. Incubation with the nuclear stain and the 20x DAPI imaging settings were identical throughout each assay. DAPI images had similar fluorescence signals throughout the course of the previously performed assays. Moreover, there was a larger fluorescence decrease of nuclei seen in HCC tissue compared to normal liver nuclei. This trend continued when observing other tissue types from the TMAs in this specific assay (Appendix, Figure A4)**.** There seemed to be a decrease in nuclear staining throughout the three arrays and more specifically, the bottom two rows (which includes the HCC tissue) looked to have a larger fluorescence decrease compared to the top two rows. This suggests the NucBlue was old or that there may have been problems during the staining procedure resulting in nonuniform staining. Nonetheless, using a NIR fluorophore did not result in any concrete findings with non-specific binding and AF remaining the biggest issues.

3.6. Autofluorescence

Although autofluorescence can cause an abundance of problems when using fluorescence imaging, there are advantages of endogenous fluorescence as well. During changes of normal bodily processes, tissue damage or pathological changes, modifications of the body's biochemical compositions and structural organization occur which leads to changes in tissue autofluorescence [51, 52]. Because of these physiological changes, autofluorescence can be monitored and used for diagnostic applications [51, 52]. For example, an AF diagnostic technique that can be used in

endoscopic detection of dysplasia, lesions, and cancer of the gastrointestinal tract is based on spectral changes of the mucosa and tissue architecture [44]. This technique can also be used in the detection of oral malignancies, also based on spectral property changes in times of pathological alteration, where even tiny changes, such as inflammation of the oral epithelium, change the fluorescence properties of tissue [53]. Autofluorescence monitoring applications can be a useful tool compared to biopsies, as it is usually a non-invasive, less expensive technique, and in many cases, can more easily detect early neoplastic changes [51].

When researching further into liver autofluorescence, a 2009 study using a 780 nm laser multiphoton imaging device, found that HCC tissue yielded lower autofluorescence intensities than normal liver, with an intensity ratio of 0.250 ± 0.20, but found no correlation in regards to HCC grade [54]. When looking at the control array used in the aptamer refolding assay, there is no obvious trend seen between uninvolved liver and HCC tissues integrated intensities (Figure 5B). However, there could be fluorophore contributing to the fluorescence signal because the tissue was stained with TLS11a/fluorescein without aptamer refolding (no negative control). Also, due to the array being FFPE, some of the autofluorescence could be attributed to formalin fixation rather than endogenous fluorescence properties which led to the inability to reach a conclusive result regarding this issue.

Other studies were found that looked at more specific autofluorescence properties of the liver including NAD(P)H of liver graft transplants, altered metabolic conditions in rat hepatocytes, and AF in different forms of liver diseases [52, 55, 56]. Interestingly, it was found that the most crucial endogenous fluorophores, which aid in distinguishing

normal liver, fibrotic and cirrhotic liver from one another, are NAD(P)H, collagen and vitamin A, respectively [52]. Additionally, it was found that normal liver tissue exhibited 50% less autofluorescence signal than fibrotic tissue and 75% less than cirrhotic liver [52]. Conclusively, these studies demonstrate the possible advantages endogenous fluorescence holds and demonstrates the ability to utilize intrinsic biomarkers for distinguishing between normal and diseased liver states for diagnostic purposes.

Granted that autofluorescence can be advantageous in the right circumstances, it created an abundance of obstacles and was viewed as more of a nuisance regarding this study. To continue this project, it was deemed necessary to find an alternative method or change directions completely. When research into which route to take, it was discovered that there are several approaches one could take to help decrease background and increase aptamer detection when using FFPE tissue arrays. The most commonly used method to decrease autofluorescence on formalin-fixed tissue is, prior to staining, using AF quenching dyes such as Sudan Black B, Trypan Blue, sodium borohydride and Eriochrome black T treatments or light irradiation [45, 57, 58]. The chemical quenching treatments have been shown to decrease autofluorescence in many different studies; however, they also can reduce the signal of the fluorescence probe, and the quenching efficacy is related to the cause of AF [58]. Irradiation with visible or UV light, photobleaching, has also been proven effective at diminishing autofluorescence and has been shown to nearly eliminate endogenous fluorescence of liver and brain tissue [58]. However, heat sensitive antigens can be negatively affected by this treatment and it can be a costly setup [58].

Other methods to reduce autofluorescence can be implemented during imaging. In

cases where the negative control AF is low, one can easily subtract the background from the stained images. Unfortunately, in many instances, this is not possible. Confocal imaging has also been shown to decrease levels of autofluorescence resulting in less bleed through reduction of probe intensity, thus providing higher resolution images. Another option is the use of spectral imaging and linear un-mixing which has been shown to effectively distinguish between autofluorescence and fluorophore fluorescence [59, 60]. When an image is captured, all contributing fluorescent light emission is added together; however, with specialized microscopes or linear un-mixing algorithm software, the resulting image can essentially be separated, thus distinguishing the probe from background AF [60, 61].

With the results obtained thus far, it was believed that the use of quenching dyes could potentially hamper the aptamer fluorescence signal further. Moreover, although spectral un-mixing has been shown to work effectively, accessible microscopes did not have such ability and the cost of purchasing the software was unfeasible. With all possible options exhausted, it was determined that the next best alternative would be trying immunohistochemistry with the use of colorimetric detection rather than fluorescence.

3.7. Colorimetric Analysis

Two 1427 TMA were used for colorimetric analysis. One array was incubated with 100 nM biotinylated TLS11a while the other array was incubated with PBSA in place of aptamer, while all other steps were identical. Images were obtained using light microscopy (Figure 10A-B). Quantitative analysis of normal and HCC tissue was performed to determine if the staining score was considered positive or negative. Similar

results were found when comparing the negative control (no aptamer) and 100 nM TLS11a stained array (Figure 10C). The resulting mean pixel intensity for normal liver was 97.92% negative, 2.08% low positive for the negative control and 98.33% negative, 1.67% low positive for the TLS11a stained array while the HCC tissue resulted in 97.97% negative, 2.03% low positive and 96.35% negative, 3.65% low positive, respectively. Neither the control or TLS11a stained arrays normal liver or HCC resulted in any positive or high positive intensity pixels and both arrays normal liver and HCC tissue resulted in an overall negative score.

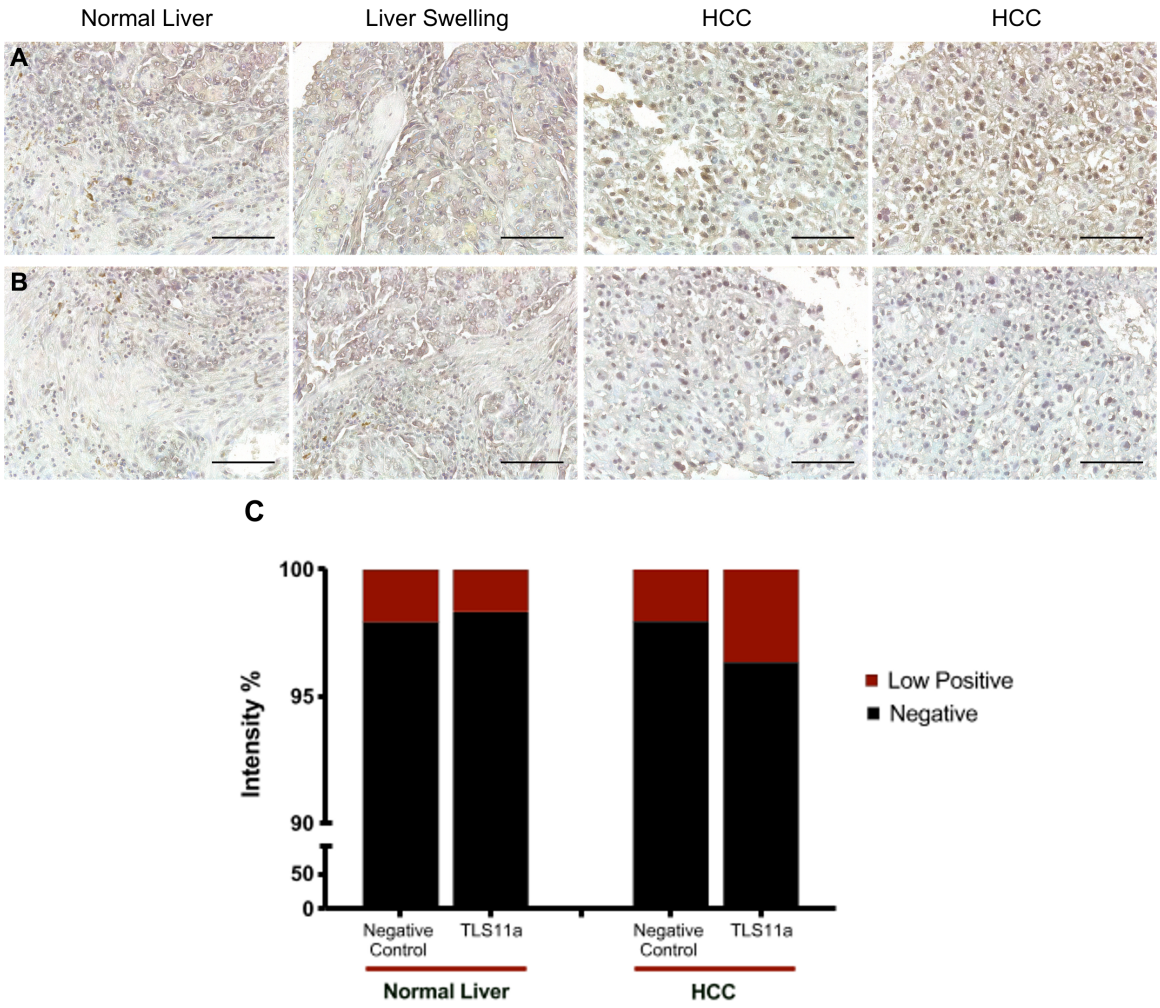

Figure 10. Immunohistochemistry assay imaged under light microscopy showing 40x images of normal liver, liver cell swelling and two HCC tissues. (A) No aptamer array (B) 100 nM biotinylated TLS11a treated array. DAB stain is seen in brown while hematoxylin nuclear stain is seen in purple. Scale bar represents 100 μm. (C) Quantitative analysis of pixel intensity, 0 to 100% were classified as negative (navy) with the max intensity being classified as low positive (red) using Image J's IHC profiler plugin.

Unable to find any conclusive results using both fluorescence and chromogenic staining methods, an alternative method was needed or the project was going to be discontinued. It is known that some antigens in FFPE tissue are not able to sustain antigenicity as well as fresh frozen tissue, even with the additional step of antigen retrieval [62] and increased storage times of formalin-fixed tissue can cause degradation

of epitopes reducing staining intensity [63, 64]. There are also some indications of decreased protein, mRNA and DNA yields in FFPE tissue as compared to that of fresh frozen tissue [65, 66]. That being the case, the last attempt was to use fresh frozen tissue in the hopes of getting more reliable results. It was thought that using fresh frozen tissue could possibly answer questions regarding loss of antigenicity due to formalin fixation and help decrease autofluorescence.

3.8. Frozen TMA Analysis

A negative control and 100 nM TLS11a/AlexaFluor-546 staining was performed on fresh frozen matched liver TMAs to see if there was a decrease in autofluorescence. If so, this assay could determine whether the aptamer could differentiate between uninvolved liver and HCC as well as HCC grade. Both 20x scans and images were obtained under identical light settings with the 20x images, set to a stack threshold, being used to gather integrated intensity measurements.

Fortunately, autofluorescence did not seem to be an issue with the fresh frozen tissue as there was no fluorescence signal observed in the RFP channel with the negative control array (Figure 11A-C). Looking at the 100 nM TLS11a/AlexaFluor-546 stained array, there was very little to no fluorescence signal observed from the uninvolved liver tissue with a mean integrated intensity of $1.77 \times 10^6 \pm 4.29 \times 10^5$ while HCC tissue gave bright red fluorescence with a mean integrated intensity of $1.92 \times 10^7 \pm 1.99 \times 10^6$. On average, the integrated intensity of HCC tissue increased more than 10-fold as compared to uninvolved liver tissue. A two-tailed Student's t-test indicated there was a significant difference between staining of uninvolved liver and HCC tissue with $p<0.0001$ ($n=40$). These results clearly demonstrate that TLS11a can successfully differentiate between

normal liver tissues and HCC tissue. No significant difference was found when comparing the integrated intensity of Grade I HCC ($2.96 \times 10^7 \pm 2.02 \times 10^6$, n=4) to the integrated intensity of Grade II HCC ($1.99 \times 10^7 \pm 2.67 \times 10^6$, n=26) (p=0.1733). However, out of the arrays' 20 total tissue cores, only two were Grade I HCC, 13 were Grade II HCC, while the remaining 5 were not graded. If there had been a larger sample size, the results may have revealed that the aptamer was better able to bind to a certain grade.

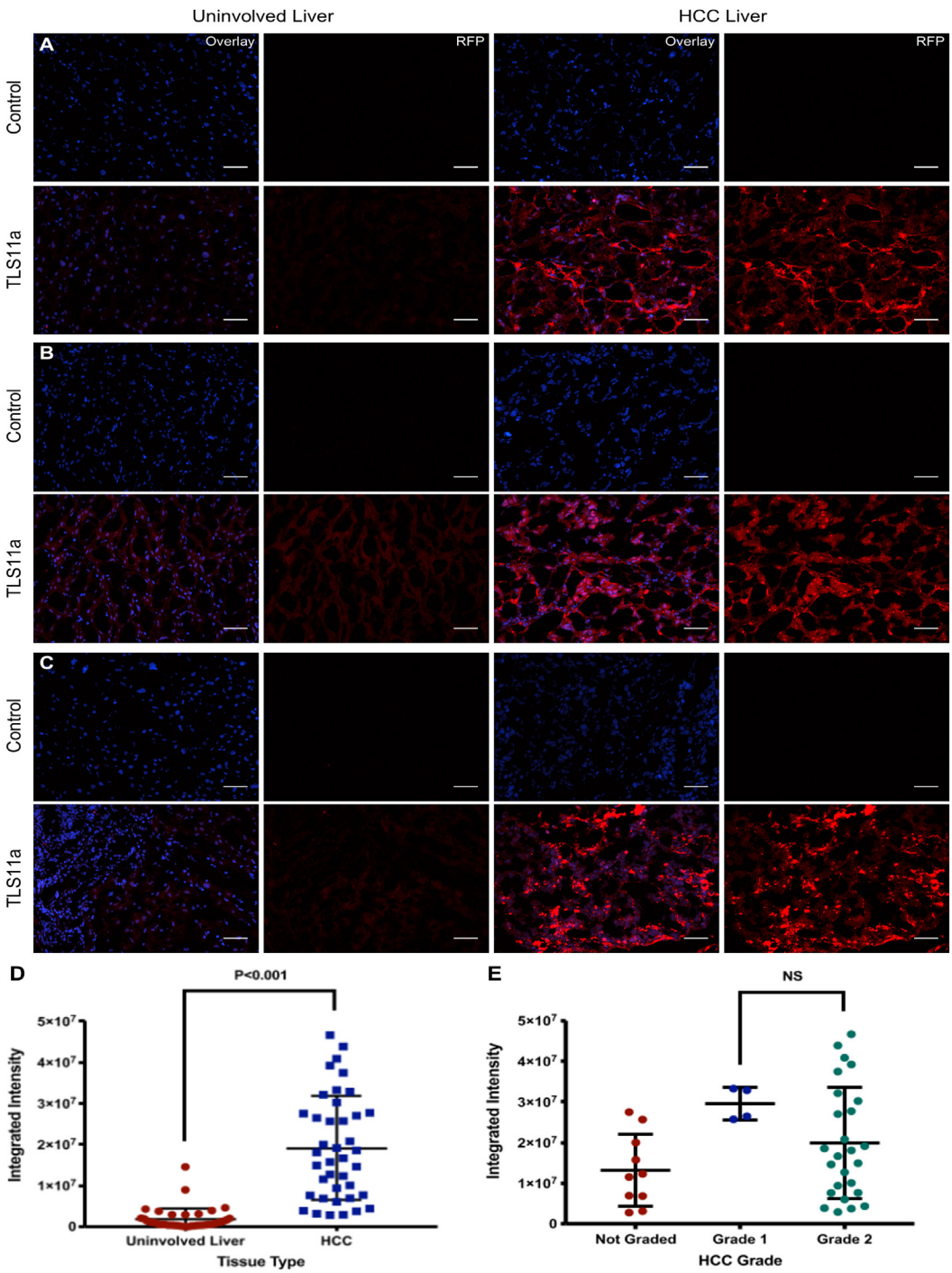

Figure 11. Fresh frozen liver tissue TMA assay. Stained with 100 nM TLS11a and no aptamer (negative control). 20x Fluorescence images of both uninvolved liver and HCC tissue, stained with NucBlue nuclei stain (blue) and TLS11a/AlexaFluor-546 (red). Images demonstrate the tissue that was closest to the mean integrated intensity for each grade, displaying both the merged and RFP channel images from the negative control TMA (top) and aptamer TMA (bottom) uninvolved liver (left two columns) and HCC tissue (right two columns) for each letter. (A) Tissue case that was Ungraded (B) HCC Grade I case (C) HCC Grade II case. Scale bar represents 100 μm. TLS11a stained TMAs integrated intensity quantitative analysis of (D) all uninvolved liver and HCC tissue and (E) HCC tissues based on Grade. $p<0.050$ was considered significant in a two-tailed Student's t-test.

To further evaluate the specificity of TLS11a, the same assay was performed on FF multi-organ TMAs. Besides scans being obtained with a 10x objective, the same methods as above were used to gather and collect measurements. Figure 12 shows the merged blue (NucBlue nuclei stain) and RFP channel (TLS11a/AlexaFluor-546) 10x scans of the complete 100 nM TLS11a stained array.

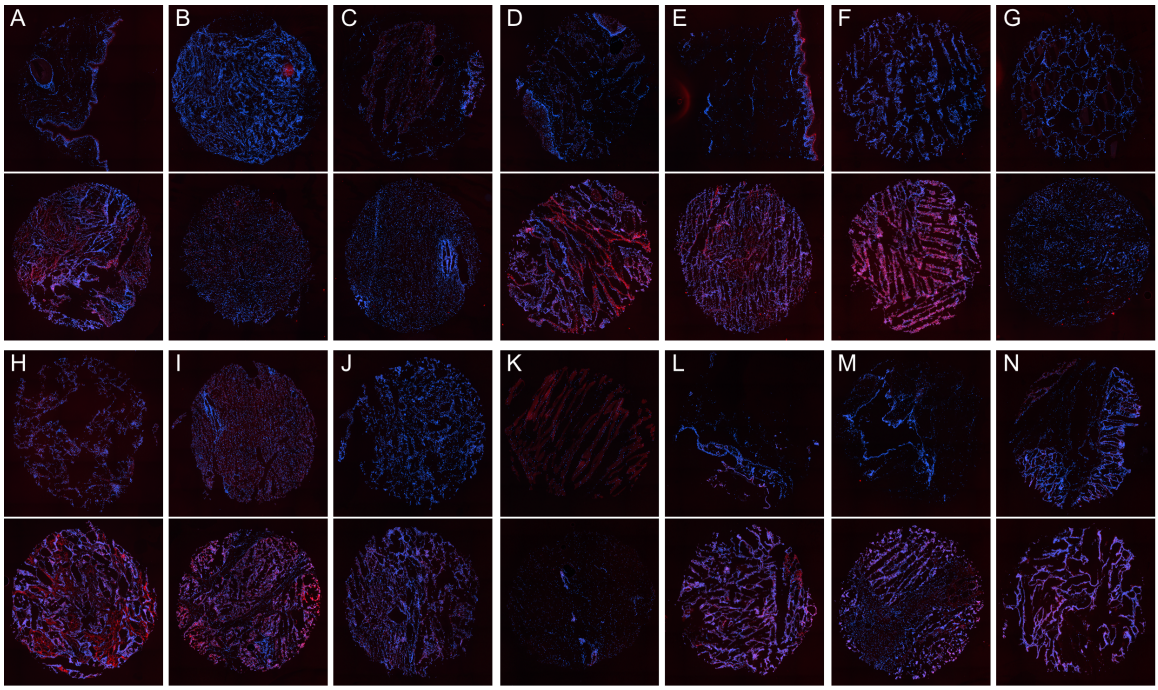

Figure 12. Fresh frozen multi-organ TMA assay. Merged 10x fluorescence scans, stained with NucBlue nuclei stain (blue) and 100 nM TLS11a/AlexaFluor-546 (red), showing each organ types (represented by a letter) normal tissue (top row) and matched malignant tissue (bottom row). (A) Vulva, (B) Ovary, (C) Stomach, (D) Esophagus, (E) Skin, (F) Testis, (G) Thyroid gland, (H) Lung, (I) Liver, (J) Kidney, (K) Skeletal muscle, (L) Colon, (M) Breast, and (N) Rectum tissues.

Looking at the 20x images, the control array displayed very little autofluorescence although many malignant tissue types displayed a low fluorescence signal (Figure 13A). To compensate for the negative control's fluorescence signal, each image was measured and subtracted from the 100 nM TLS11a stained. Most the non-malignant normal tissue

showed very little to no increase of integrated intensity and demonstrated very little fluorescence signal when compared to that of the negative control (Figure 13B); however, the stomach, colon, and rectum did show a small increase in both integrated intensity and fluorescence signal. A one-way ANOVA followed by Holm-Sidak post hoc test of integrated intensity of all normal tissues and the integrated intensity of HCC indicated there was a significant difference with $p<0.0001$ for all normal tissues, including normal liver. A one-way ANOVA followed by Holm-Sidak post hoc test determined there was a significant difference between the liver integrated intensities ratio and other tissue types ratio (Figure 13C) ($p<0.05$) although, TLS11a did show a large degree of labeling in multiple malignant tissue types relative to their matched normal tissue. Some malignant tissues demonstrated more labeling relative to its matched normal tissue, most notably in HCC, testis, rectum, esophagus, lung and colon tissues, when compared to the negative controls (Figure 13D). These results demonstrate that TLS11a has the potential to be a tumor-specific marker, especially in respect to HCC, demonstrating a high degree of labeling in multiple malignant tissue types.

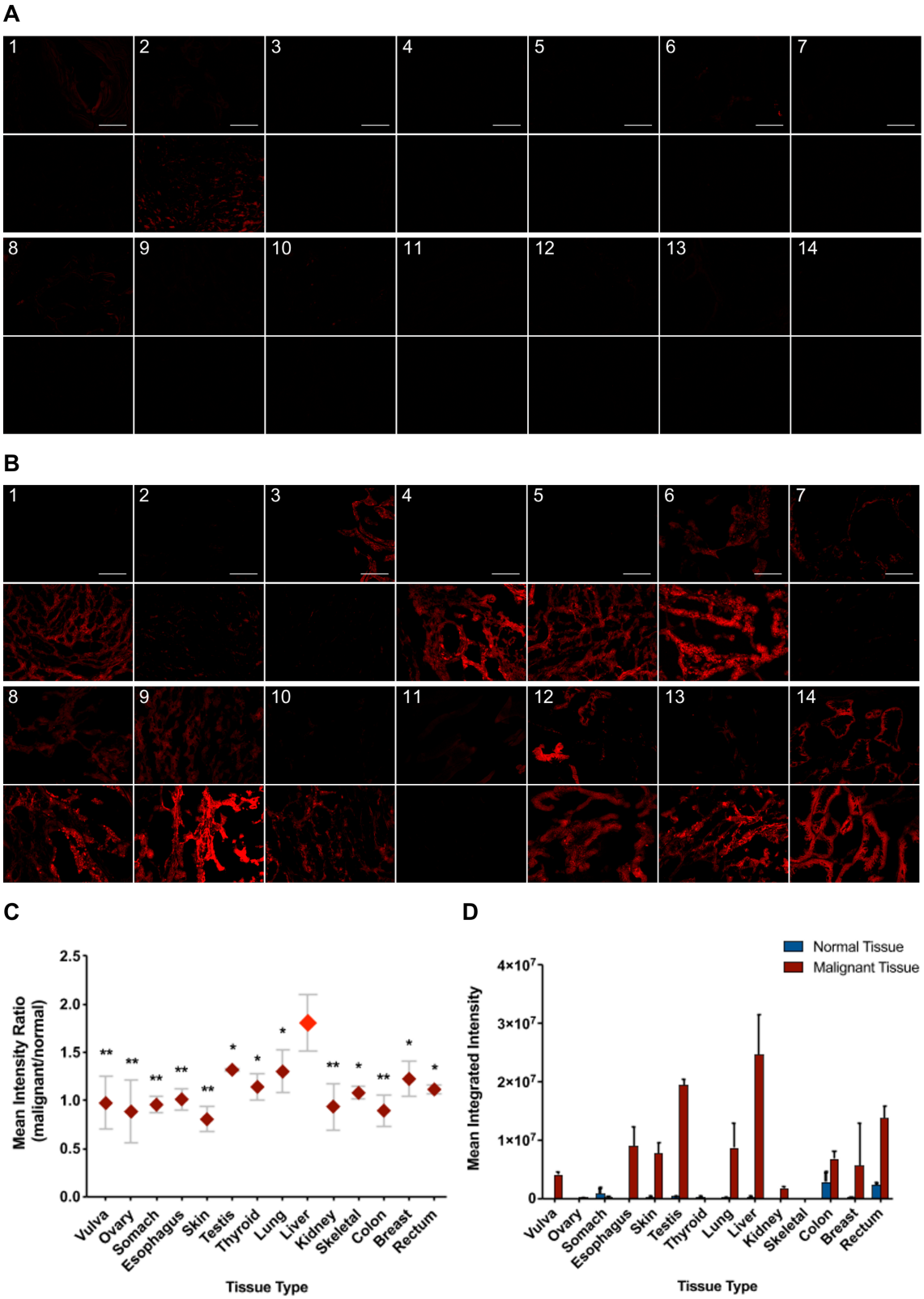

Figure 13. Fresh frozen multi-organ TMA 20x RFP channel images. The (A) Negative control and (B) 100 nM TLS11a/AlexaFluor-546 TMA show (1) Vulva, (2) Ovary, (3) Stomach, (4) Esophagus, (5) Skin, (6) Testis, (7) Thyroid Gland, (8) Lung, (9) Liver, (10) Kidney, (11) Skeletal Muscle, (12) Colon,

Figure 13. (continued) (13) Breast, and (14) Rectum with the top row being normal and the bottom row being malignant tissue for A and B. Scale bar represents 100 μm. (C) Mean intensity ratio (malignant/normal) quantitative analysis with $p > 0.05$ being considered significant. (D) Mean integrated intensity of both the normal (blue) and malignant (red) tissue from each tissue type.

4. CONCLUSION

In this thesis, the specificity of TLS11a, a previously discovered aptamer that has shown to be HCC-specific in MEAR cells, towards human HCC cells was examined by performing IHC analysis on multiple types of TMAs. The intensity of TLS11a/AlexaFluor-546 stained formalin-fixed tissues were compared to identically treated negative controls which resulted in the negative control TMA demonstrating similar, and in some cases higher, fluorescence signal than the aptamer stained arrays. Attempts were made to try and unmask epitopes with antigen retrieval and ensure the aptamer was in a stable secondary structure with aptamer refolding. Also, it was speculated that changing fluorophores from AlexaFluor-546 to fluorescein would decrease autofluorescence and give better results. When this approach failed, the switch to indirect staining with AlexaFluor-750 was attempted in hopes that it would both amplify the signal and nearly diminish autofluorescence imaging at longer wavelengths. Still, a strong autofluorescence was seen over a 480-750 nm wavelength range, or in the case of the indirect staining assay, non-specific binding became an issue. This made it extremely difficult, if not impossible, to distinguish our target fluorescence from tissue autofluorescence, thus decreasing the ability to perform further immunofluorescence staining on FFPE tissues.

Furthermore, preliminary results obtained prior to the control assays, are inaccurate and is probable that most of the fluorescence signal was autofluorescence. TMAs were also imaged using confocal microscopy (data not shown) to try and remove AF; however, it proved to be unproductive, resulting in similar findings. Formalin-fixed TMA colorimetric assays were performed to try and move away from fluorescence;

however, these resulted in the same problems seen with fluorescence with the negative controls exhibiting comparable results as the aptamer stained arrays.

Fortunately, fresh frozen TMAs exhibited very little autofluorescence from the negative control. Fresh frozen aptamer staining revealed TLS11a could recognize and differentiate between human normal liver and HCC, resulting in more than an average 10-fold binding increase, with little to no binding seen in normal liver tissue. No correlation was found in TLS11a's ability to differentiate between HCC with different grades; however, a further analysis with a larger sample size is needed to confirm this hypothesis. Furthermore, a very low degree of binding was seen in the normal tissue of 19 other normal tissue types tested. Results indicated there was a notable amount of labeling in many malignant tissue types' suggesting that TLS11a could potentially function as a multi tumor-specific marker; however, more labeling was seen in HCC relative to other malignant tissue types suggesting a selectivity towards HCC tissues.

Additionally, the fact that fresh frozen assays could provide conclusive results but both fluorescence and colorimetric staining of formalin-fixed tissue could not be is important. This data suggests that the epitope TLS11a targets is destroyed in the formalin fixation process. It was believed that there the autofluorescence was masking TLS11a probes fluorescence, however, results from the IHC assays demonstrated similar finding with no aptamer signal being detected. IHC is an alternative method researchers use when fluorescence is not an option, and the fact that neither assay worked contributes to the idea that fixation destroys this epitope. Although, the specific TLS11a target is unknown, studies currently being conducted suggest it is the extracellular domain of a membrane protein. Membrane proteins are the most vulnerable and exposed during the fixation

process; it may be possible that the harsh methods used for fixation destroy TLS11a's target antigen. Consequently, additional research should be limited to the use of fresh frozen tissue rather than Formalin fixed tissue. Furthermore, TLS11a recognizing multiple malignant tissue types suggest that its target ligand may be some type of cell surface growth factor receptor or some protein that has low expression in normal tissues but is highly over-expressed in malignant tissues. Future research could use this information to identify TLS11a's target epitope.

Ultimately, this research indicates that TLS11a has the potential to target multiple human malignant tissue types with a significant preference towards HCC tissue *in situ*. TLS11a has the potential to be used not only as a tumor-specific marker but also a HCC targeting molecule that could be utilized in diagnostic or drug targeting applications. Previous studies have shown TLS11a effective at targeted-drug delivery to MEAR cells *in vitro* and, combined with these finding, suggest TLS11a has the potential to be the HCC-targeting marker that is needed to help decrease HCC incidence and mortality rates worldwide.

APPENDIX SECTION

Example ROI's used to measure the mean fluorescence intensity of scanned 8- bit images. Images were first subject to background removal and then multiple ROI's were created and measured. The same ROIs were used for all tissue core scan on the same array and on arrays that were being used for comparison.

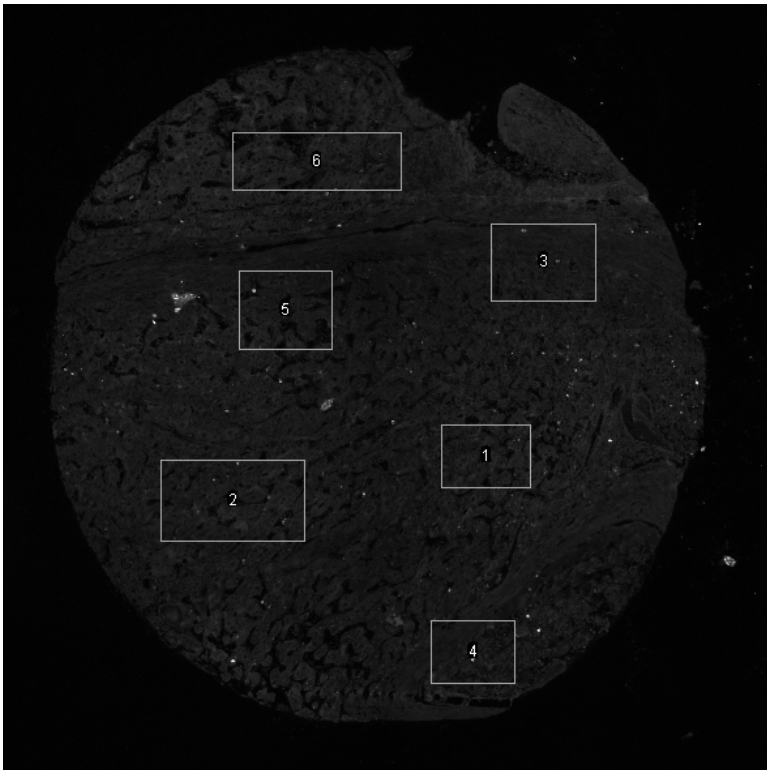

Figure A1. Multiple ROI measurement of scanned tissue core images.

Method used to create a threshold, identical for all images in a stack, for measuring 20x or 40x images. Measurements are limited to threshold to ensure only pixels above the determined threshold are counted. Figure A2 shows the 8-bit stack prior to threshold (A), how the threshold is determined, based off a stack histogram (B), the image set at the determined stack histogram threshold (C) and the measurements needed for analysis (D).

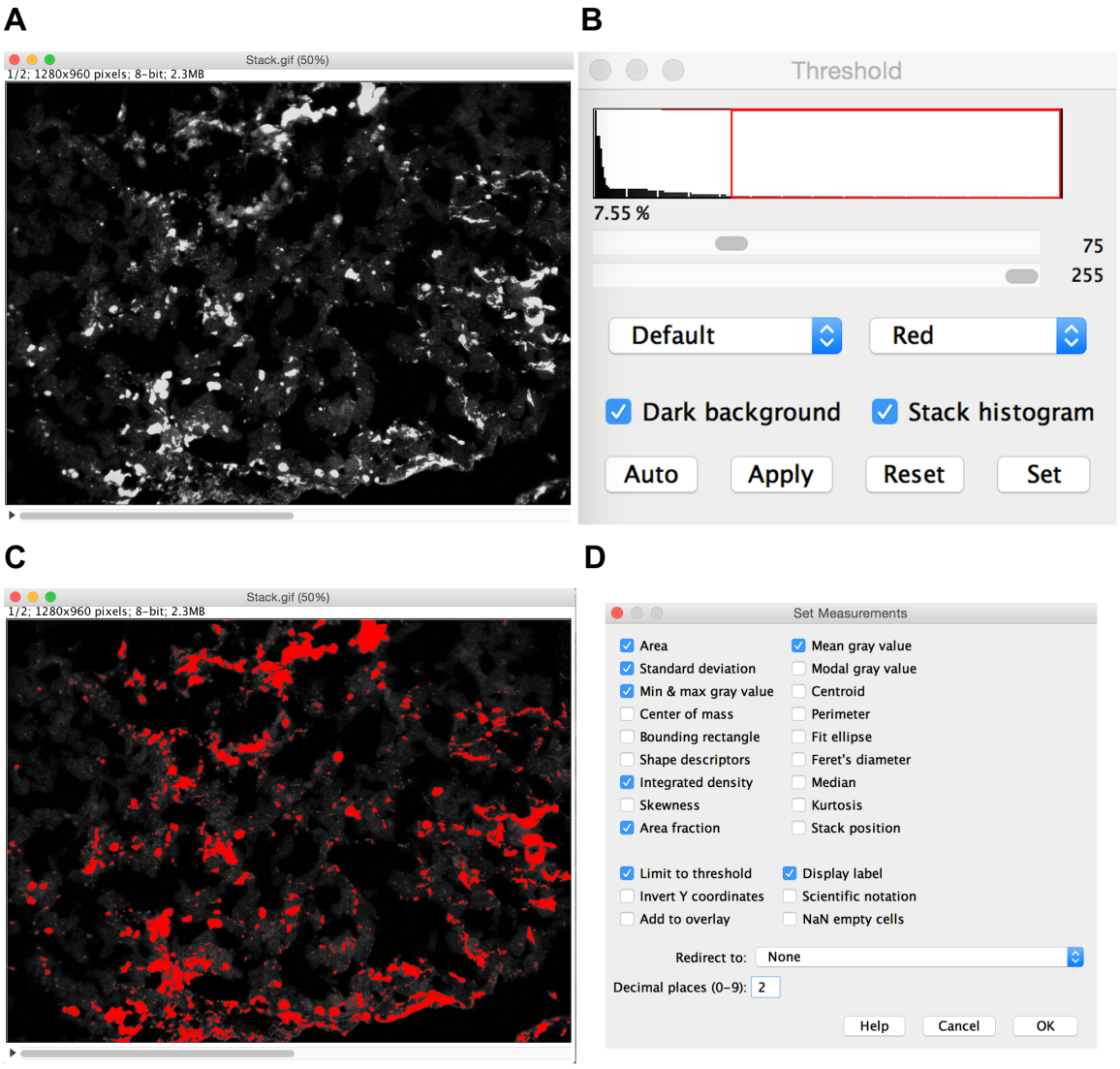

Figure A2. Stack threshold example. (A) Original 8-bit image stack (B) Threshold tool used to determine stack threshold (C) Stack images after threshold (D) Measurements selected for analysis of images.

Method used to analyze colorimetric images stained with biotinylated TLS11a. Method performed using IHC Profiler, an Image J plugin, that scores the image staining as positive or negative and classifies pixel intensities into negative, low positive, positive and high positive groups for reference.

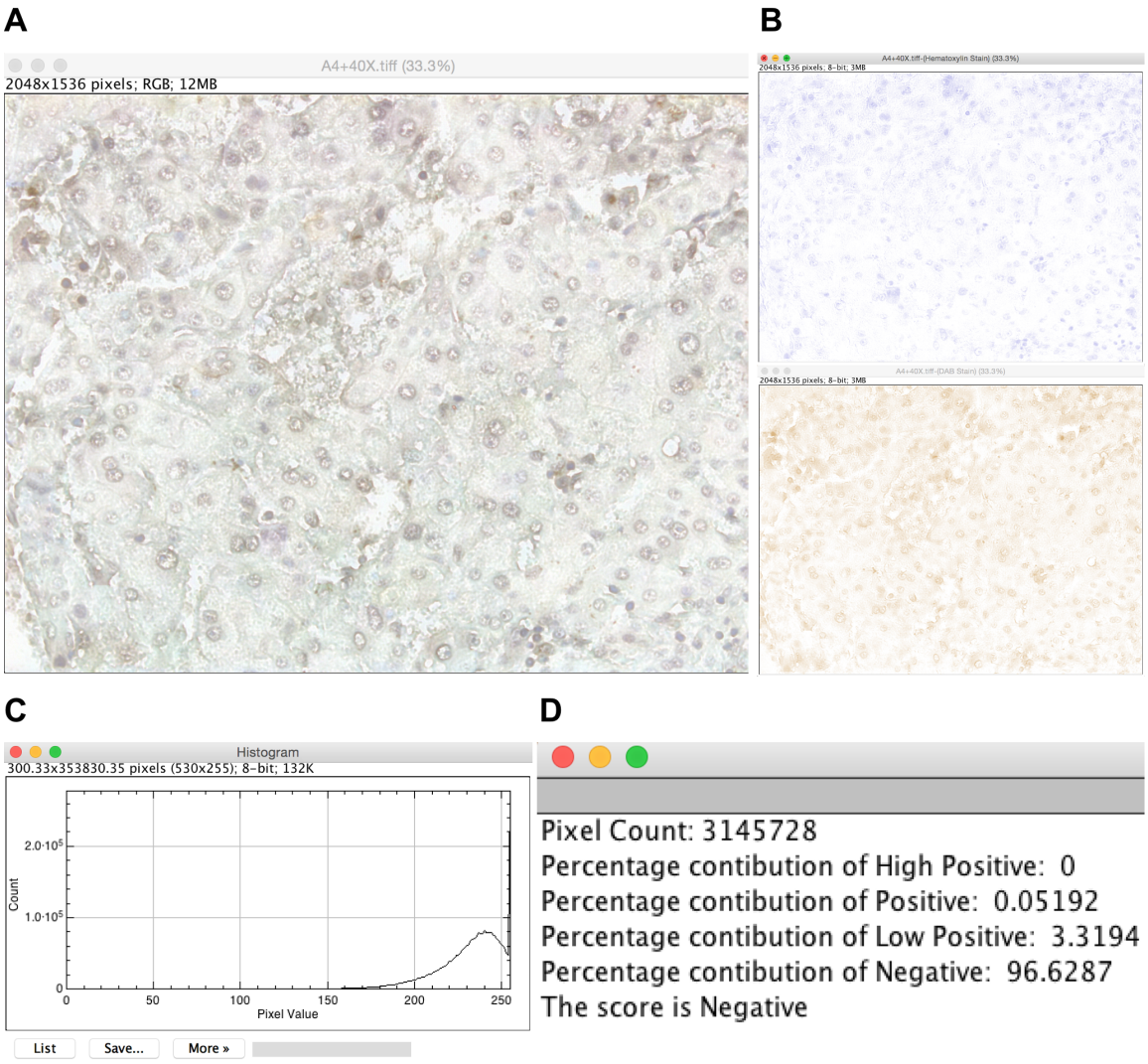

Figure A3. Colorimetric analysis using IHC Profiler plugin. (A) Original 20x light microscopy image (B) Example of how IHC separates the image into hematoxylin (top) and DAB (bottom) stains (C) Resulting histogram of the DAB image pixels (D) Resulting table of information provided about the DAB image score and breakdown of pixel groups.

DAPI channel images from the indirect staining assays 100 nM TLS11a stained array compared to an alternate assays DAPI channel images, imaged under identical settings, of the same tissues. Images demonstrate a significant decrease in DAPI fluorescence suggesting the stain was old or problems with the staining procedure.

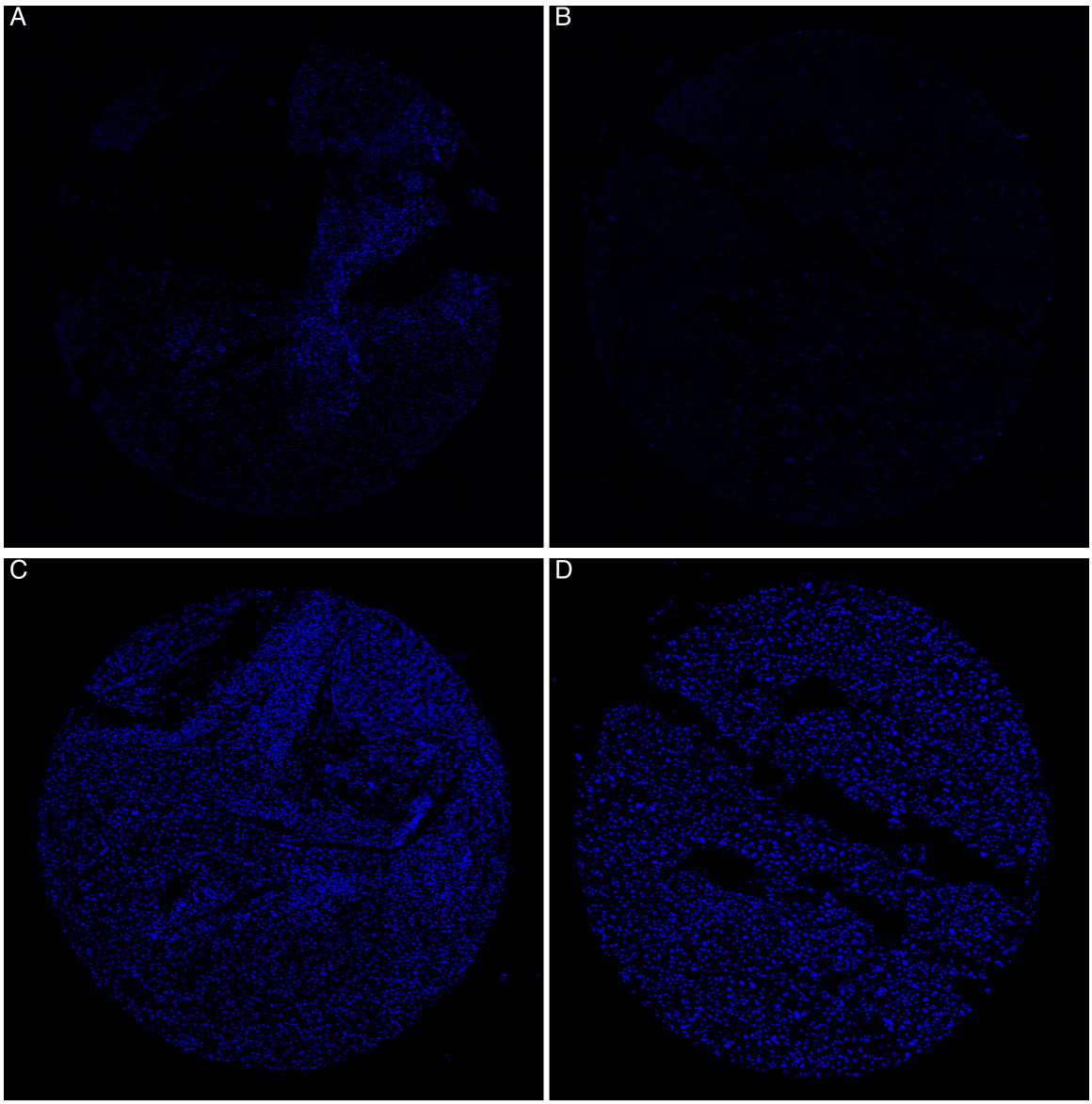

Fig**ure A4.** 20x scanned tissue core from the DAPI channel using identical image acquisition settings. A & B are from the indirect staining assay of the 100 nM TLS11a stained array (A) Normal liver (B) HCC. The same tissue cores from a previously stained 100 nM TLS11a during a previous assay (C) Normal liver (D) HCC.

LITERATURE CITED

1. American Cancer Society, *Cancer Facts and Figures 2015*. 2015: Atlanta.
2. Siegel, R.L., K.D. Miller, and A. Jemal, *Cancer statistics, 2016.* CA: A Cancer Journal for Clinicians, 2016. **66**(1): p. 7-30.
3. Shangguan, D., et al., *Identification of Liver Cancer-Specific Aptamers Using Whole Live Cells.* Analytical Chemistry, 2008. **80**(3): p. 721-728.
4. Amercian Cancer Society, *Cancer Facts and Figures 2016*. 2016: Atlanta.
5. Ferlay, J., et al., *Cancer incidence and mortality worldwide: sources, methods and major patterns in GLOBOCAN 2012.* Int J Cancer, 2015. **136**(5): p. E359-86.
6. Anand, P., et al., *Cancer is a Preventable Disease that Requires Major Lifestyle Changes.* Pharmaceutical Research, 2008. **25**(9): p. 2097-2116.
7. Kathleen Collins, T.J., Nikola P. Pavletich, *The cell cycle and cancer.* PNAS, 1997. **94**(7): p. 2776-2778.
8. Harvey Lodish, A.B., S Lawrence Zipursky, Paul Matsudaira, David Baltimore, and James Darnell, *Checkpoints in Cell-Cycle Regulation*, in *Molecular Cell Biology*. 2000, W.H. Freeman: New York.
9. Sager, R., *Genetic Suppression of Tumor Formation: A New Frontier in Cancer Research.* Cancer Research, 1986. **46**(4 Part 1): p. 1573.
10. Hanahan, D. and R.A. Weinberg, *Hallmarks of cancer: the next generation.* Cell, 2011. **144**(5): p. 646-74.
11. Attwa, M.H. and S.A. El-Etreby, *Guide for diagnosis and treatment of hepatocellular carcinoma.* World J Hepatol, 2015. **7**(12): p. 1632-51.
12. Frederick L, G., et al., *AJCC Cancer Staging Manual*. Ajcc Cancer Staging Manual. 2002: Springer New York.
13. Grisham, J.W., *Organizational Principles of the Liver*, in *The Liver*. 2009, John Wiley & Sons, Ltd. p. 1-15.
14. Ryerson, A.B., et al., *Annual Report to the Nation on the Status of Cancer, 1975-2012, featuring the increasing incidence of liver cancer.* Cancer, 2016. **122**(9): p. 1312-1337.
15. Forner, A., J.M. Llovet, and J. Bruix, *Hepatocellular carcinoma.* The Lancet, 2012. **379**(9822): p. 1245-1255.
16. Dhanasekaran, R., A. Limaye, and R. Cabrera, *Hepatocellular carcinoma: current trends in worldwide epidemiology, risk factors, diagnosis, and therapeutics.* Hepatic Medicine : Evidence and Research, 2012. **4**: p. 19-37.
17. Knox, J.J., S.P. Cleary, and L.A. Dawson, *Localized and systemic approaches to treating hepatocellular carcinoma.* J Clin Oncol, 2015. **33**(16): p. 1835-44.
18. Cho, E.J., J.W. Lee, and A.D. Ellington, *Applications of aptamers as sensors.* Annu Rev Anal Chem (Palo Alto Calif), 2009. **2**: p. 241-64.
19. Ellington, A.D. and J.W. Szostak, *In vitro selection of RNA molecules that bind specific ligands.* Nature, 1990. **346**(6287): p. 818-22.
20. Jayasena, S.D., *Aptamers: An Emerging Class of Molecules That Rival Antibodies in Diagnostics.* Clinical Chemistry, 1999. **45**(9): p. 1628-1650.
21. Stoltenburg, R., C. Reinemann, and B. Strehlitz, *SELEX--a (r)evolutionary method to generate high-affinity nucleic acid ligands.* Biomol Eng, 2007. **24**(4): p. 381-403.

22. Chen, H., et al., *MUC1 Aptamer-Based Near-Infrared Fluorescence Probes for Tumor Imaging.* Molecular Imaging and Biology, 2015. **17**(1): p. 38-48.
23. Ferreira, C.S., S. Matthews Cs Fau - Missailidis, and S. Missailidis, *DNA aptamers that bind to MUC1 tumour marker: design and characterization of MUC1-binding single-stranded DNA aptamers.* (1010-4283 (Print)).
24. Powell Gray, B., et al., *Abstract 5523: A novel aptamer targeting agent for prostate cancer.* Cancer Research, 2015. **75**(15 Supplement): p. 5523.
25. Gobbo, J., et al., *Restoring Anticancer Immune Response by Targeting Tumor-Derived Exosomes With a HSP70 Peptide Aptamer.* Journal of the National Cancer Institute, 2016. **108**(3).
26. Sun, D., et al., *A repeatable assembling and disassembling electrochemical aptamer cytosensor for ultrasensitive and highly selective detection of human liver cancer cells.* Anal Chim Acta, 2015. **885**: p. 166-73.
27. Sun, D., et al., *Sensitive electrochemical aptamer cytosensor for highly specific detection of cancer cells based on the hybrid nanoelectrocatalysts and enzyme for signal amplification.* Biosens Bioelectron, 2016. **75**: p. 301-7.
28. Kashefi-Kheyrabadi, L., et al., *Ultrasensitive Detection of Human Liver Hepatocellular Carcinoma Cells Using a Label-Free Aptasensor.* Analytical Chemistry, 2014. **86**(10): p. 4956-4960.
29. Mohseni, H., et al., *Targeting hepatocellular carcinoma with aptamer-functionalized PLGA/PLA-PEG nanoparticles.* 2014. **9166**: p. 916605.
30. Shannon E. Weigum, E.M., Christopher Munoz, Richard Feng, Travis Cantu, Kyle Walsh, Tania Betancourt, *Targeted therapy of hepatocellular carcinoma with aptamer-functionalized biodegradable nanoparticles.* Journal of Nanoparticle Research, 2016. **18**(341).
31. Kononen, J., et al., *Tissue microarrays for high-throughput molecular profiling of tumor specimens.* Nat Med, 1998. **4**(7): p. 844-847.
32. Packeisen, J., et al., *Tissue microarrays: a new approach for quality control in immunohistochemistry.* J Clin Pathol, 2002. **55**(8): p. 613-5.
33. Wang, H., et al., *Tissue Microarrays: Applications in Neuropathology Research, Diagnosis, and Education.* Brain Pathology, 2002. **12**(1): p. 95-107.
34. Dolled-Filhart, M.P. and M.D. Gustavson, *Tissue microarrays and quantitative tissue-based image analysis as a tool for oncology biomarker and diagnostic development.* Expert Opinion on Medical Diagnostics, 2012. **6**(6): p. 569-583.
35. Kokolakis, G., et al., *From the protein to the graph: How to quantify immunohistochemistry staining of the skin using digital imaging.* Journal of Immunological Methods, 2008. **331**(1–2): p. 140-146.
36. Kirkeby, S. and C.E. Thomsen, *Quantitative immunohistochemistry of fluorescence labelled probes using low-cost software.* Journal of Immunological Methods, 2005. **301**(1–2): p. 102-113.
37. Varghese, F., et al., *IHC Profiler: An Open Source Plugin for the Quantitative Evaluation and Automated Scoring of Immunohistochemistry Images of Human Tissue Samples.* PLOS ONE, 2014. **9**(5): p. e96801.
38. Zuker, M., *Mfold web server for nucleic acid folding and hybridization prediction.* Nucleic Acids Research, 2003. **31**(13): p. 3406-3415.
39. Dako, *Immunohistochemical Staining Methods*. 2013.

40. Cattoretti, G., et al., *Antigen unmasking on formalin-fixed, paraffin-embedded tissue sections.* The Journal of Pathology, 1993. **171**(2): p. 83-98.
41. Pileri, S.A., et al., *Antigen retrieval techniques in immunohistochemistry: comparison of different methods.* The Journal of Pathology, 1997. **183**(1): p. 116-123.
42. Hermanson, G.T., *Bioconjugate Techniques*. 3rd ed. 2013, Amsterdam: Acad. Press.
43. Watt, R.M. and E.W. Voss Jr, *Mechanism of quenching of fluorescein by anti-fluorescein IgG antibodies.* Immunochemistry, 1977. **14**(7): p. 533-541.
44. Haringsma, J. and G.N.J. Tytgat, *Fluorescence and autofluorescence.* Best Practice & Research Clinical Gastroenterology, 1999. **13**(1): p. 1-10.
45. Viegas, M.S., et al., *An improved and cost-effective methodology for the reduction of autofluorescence in direct immunofluorescence studies on formalin-fixed paraffin-embedded tissues.* (1121-760X (Print)).
46. Croce, A.C. and G. Bottiroli, *Autofluorescence Spectroscopy and Imaging: A Tool for Biomedical Research and Diagnosis.* European Journal of Histochemistry : EJH, 2014. **58**(4): p. 2461.
47. Frangioni, J.V., *In vivo near-infrared fluorescence imaging.* Current Opinion in Chemical Biology, 2003. **7**(5): p. 626-634.
48. Sevick-Muraca, E.M., J.P. Houston, and M. Gurfinkel, *Fluorescence-enhanced, near infrared diagnostic imaging with contrast agents.* Current Opinion in Chemical Biology, 2002. **6**(5): p. 642-650.
49. Jiang, W., et al., *Assessing Near-Infrared Quantum Dots for Deep Tissue, Organ, and Animal Imaging Applications.* JALA: Journal of the Association for Laboratory Automation, 2008. **13**(1): p. 6-12.
50. Buchwalow, I., et al., *Non-specific binding of antibodies in immunohistochemistry: fallacies and facts.* Scientific Reports, 2011. **1**: p. 28.
51. Monici, M., *Cell and tissue autofluorescence research and diagnostic applications*, in *Biotechnology Annual Review*. 2005, Elsevier. p. 227-256.
52. Croce, A.C., et al., *Human liver autofluorescence: an intrinsic tissue parameter discriminating normal and diseased conditions.* Lasers Surg Med, 2010. **42**(5): p. 371-8.
53. Pavlova, I., et al., *Understanding the Biological Basis of Autofluorescence Imaging for Oral Cancer Detection: High-Resolution Fluorescence Microscopy in Viable Tissue.* Clinical Cancer Research, 2008. **14**(8): p. 2396.
54. Hovhannisyan, V., *Label-free diagnosis of human hepatocellular carcinoma by multiphoton autofluorescence microscopy.* Applied Physics Letters, 2009. **95**(19): p. 193703.
55. Castro-e-Silva, O., et al., *Autofluorescence Spectroscopy in Liver Transplantation: Preliminary Results From a Pilot Clinical Study.* Transplantation Proceedings. **40**(3): p. 722-725.
56. Croce, A.C., et al., *Autofluorescence properties of isolated rat hepatocytes under different metabolic conditions.* 2004(1474-905X (Print)).
57. Davis, A.S., et al., *Characterizing and Diminishing Autofluorescence in Formalin-fixed Paraffin-embedded Human Respiratory Tissue.* J Histochem Cytochem, 2014. **62**(6): p. 405-423.

58. Neumann, M. and D. Gabel, *Simple Method for Reduction of Autofluorescence in Fluorescence Microscopy.* Journal of Histochemistry & Cytochemistry, 2002. **50**(3): p. 437-439.
59. Chorvat, D., Jr., et al., *Spectral Unmixing of Flavin Autofluorescence Components in Cardiac Myocytes.* Biophysical Journal. **89**(6): p. L55-L57.
60. Stack, E.C., et al., *Multiplexed immunohistochemistry, imaging, and quantitation: a review, with an assessment of Tyramide signal amplification, multispectral imaging and multiplex analysis.* Methods, 2014. **70**(1): p. 46-58.
61. Zimmermann, T., J. Rietdorf, and R. Pepperkok, *Spectral imaging and its applications in live cell microscopy.* FEBS Letters, 2003. **546**(1): p. 87-92.
62. Yamashita, S. and Y. Okada, *Application of Heat-induced Antigen Retrieval to Aldehyde-fixed Fresh Frozen Sections.* Journal of Histochemistry & Cytochemistry, 2005. **53**(11): p. 1421-1432.
63. Ramos-Vara, J.A., et al., *Immunohistochemical Evaluation of the Effects of Paraffin Section Storage on Biomarker Stability.* Veterinary Pathology, 2013. **51**(1): p. 102-109.
64. Fergenbaum, J.H., et al., *Loss of Antigenicity in Stored Sections of Breast Cancer Tissue Microarrays.* Cancer Epidemiology Biomarkers & Prevention, 2004. **13**(4): p. 667.
65. Cox, M.L., et al., *Investigating fixative-induced changes in RNA quality and utility by microarray analysis.* Experimental and Molecular Pathology, 2008. **84**(2): p. 156-172.
66. Sprung, R.W., et al., *Equivalence of Protein Inventories Obtained from Formalin-fixed Paraffin-embedded and Frozen Tissue in Multidimensional Liquid Chromatography-Tandem Mass Spectrometry Shotgun Proteomic Analysis.* Molecular & Cellular Proteomics, 2009. **8**(8): p. 1988-1998.